Research Square

Preprints are preliminary reports that have not undergone peer review.
They should not be considered conclusive, used to inform clinical practice,
or referenced by the media as validated information.

High-resolution spatial transcriptomic sequencing delineates the spatial atlas of dental pulp aging

Jianmao Zheng

zhengjm25@mail.sysu.edu.cn

Sun Yat Sen Univ, Guangdong Prov Key Lab Stomatol, Guangzhou, Guangdong, Peoples R China

Fengyuan Zhang

Guanghua School of Stomatology, Sun Yat-sen University https://orcid.org/0009-0002-0018-1772

Jiayi Wang

Sun Yat-sen university

Manlin Xu

Sun Yat-sen university

Xiaobin Fu

Sun Yat-sen university

Jiyuan Zuo

Stomatology Hospital of Guangzhou Medical University

Qining Guo

Sun Yat-sen university

Qianzhou Jiang

Stomatology Hospital of Guangzhou Medical University

Junqi Ling

Guanghua School of Stomatology, Sun Yat-sen University

Yuanyuan Kong

Stomatology Hospital of Guangzhou Medical University

Article

Keywords: dental pulp aging, spatial transcriptomics, Visium HD, cellular senescence, regeneration, cell–cell interaction

Posted Date: November 18th, 2026

DOI: https://doi.org/10.21203/rs.3.rs-11345606/v1

License: This work is licensed under a Creative Commons Attribution 4.0 International License.
Read Full License

Additional Declarations: There is no conflict of interest

High-resolution spatial transcriptomic sequencing delineates the spatial atlas of dental pulp aging

*Fengyuan Zhang [1, #], Yuanyuan Kong [2, #], Jiayi Wang [1], Manlin Xu [1], Xiaobin Fu [1], Jiyuan Zuo [2], Qining Guo [1], Qianzhou Jiang [2], Junqi Ling [1, *], Jianmao Zheng [1, *]*

[1]Guanghua School of Stomatology, Hospital of Stomatology, Sun Yat-sen University, Guangdong Provincial Key Laboratory of Stomatology, Guangzhou, 510080, China.
[2]Department of Endodontics, Affiliated Stomatology Hospital of Guangzhou Medical University, Guangdong Engineering Research Center of Oral Restoration and Reconstruction, Guangzhou, 510182 Guangdong, China.

** Corresponding authors. E-mail addresses:* zhengjm25@mail.sysu.edu.cn (Jianmao Zheng), lingjq@mail.sysu.edu.cn (Junqi Ling)

[#] *Contributed equally to this work*

Keywords: dental pulp aging, spatial transcriptomics, Visium HD, cellular senescence, regeneration, cell–cell interaction

Abstract

Aging induces profound degenerative changes in dental pulp, yet its spatial molecular basis remains unclear. Here we performed Visium HD spatial transcriptomics on healthy pulp tissues from three young (18–34 years) and three aged (≥60 years) donors to map the high-resolution spatial transcriptomic landscape of pulp aging. We identified eight major cell populations and found that aged pulp exhibited a pro-inflammatory and pro-fibrotic shift, with broad suppression of vasculature development, biomineralization, and regenerative programs. The fibroblast subcluster (high *SERPINA3*/*DEPP1*) was markedly reduced, with parallel reductions in progenitor (high *SERPINA3*/*SOCS3*) and endothelial (high *ACTG2*/*PLN*) subclusters, all sharing enrichment of extracellular exosome and apoptotic pathways. Neural cells showed mild stress responses, while immune remodeling featured monocyte/macrophage reduction and plasma cell increase. Senescence-associated gene overlap identified 14 candidates, revealing downregulation of protective genes (e.g., *SOD2*, *TNFAIP3*) and upregulation of pro-inflammatory/pro-apoptotic genes (e.g., *CXCL8*, *NGFR*). Furthermore, spatial interaction analysis suggested that intercellular communication was markedly weakened in aged pulp, with reduced *MPZ–MPZ* interactions between neural cells and altered *PTN–SDC3* and *COL1A2–CD44* patterns. These findings provide the first spatial molecular framework of pulp aging, revealing that coordinated loss of pro-regenerative subclusters and emergence of a pro-inflammatory microenvironment critically compromise pulp vitality, and offering an exploratory basis for targeted therapies.

INTRODUCTION

Dental pulp is a finely structured and complex loose connective tissue that performs critically important formative, sensory, nutritive, defensive, and reparative functions. It is completely surrounded by rigid dentin and enamel externally and communicates with the outside only through the narrow apical foramen. This unique anatomical configuration renders it particularly sensitive to the cumulative effects of biological aging[1,2].

Epidemiological data indicate that the global population is undergoing an unprecedented demographic shift toward older age, and it is projected that by 2050, individuals aged ≥65 years will account for more than 16% of the global population[3]. With advancing age, the dental pulp undergoes a series of degenerative changes, including progressive deposition of secondary and tertiary dentin leading to narrowing of the pulp chamber and root canals, a marked reduction in cell numbers, aggravated collagen fibrosis, decreased vascular and nerve distribution, and a substantial loss of regenerative potential of dental pulp-derived mesenchymal stem cells, among others[4,5]. This not only severely impairs the inherent regenerative, defensive, and reparative capacity of the pulp but also results in a significantly lower success rate of vital pulp therapy (especially direct pulp capping) in aged pulp compared with young pulp[6], while greatly increasing the risk of procedural

complications such as instrument separation and ledge formation during subsequent clinical treatment (root canal therapy)[7]. This therapeutic dilemma of aging pulp poses a tremendous challenge to clinicians.

To address this therapeutic dilemma, it is necessary to further understand the spatial molecular mechanisms of dental pulp aging. In recent years, studies based on traditional bulk transcriptome sequencing[8] and single-cell RNA sequencing[9] have identified age-related gene expression changes in dental pulp tissue. Although these studies provide a certain amount of information, they cannot preserve the original spatial information of pulp tissue due to technical limitations, which consequently prevents the acquisition of spatial alterations in aging dental pulp. Currently, platforms represented by 10× Genomics Visium HD enable transcriptome-wide analysis of tissues at near-cellular high resolution (8 × 8 μm) while preserving tissue architecture. This technology has been widely applied to studies of various organs and diseases, including the liver, oral tissues, and tumors, and has revolutionized the research paradigm for complex tissues[10–14]. To date, no study has applied spatial transcriptomics to systematically compare young and aged pulp, nor have the spatial transcriptomic changes accompanying pulp aging been elucidated.

In this study, we performed comprehensive, exploratory spatial transcriptomic analysis on three healthy young and three healthy aged human pulp tissues, combined with histological validation, cell differential analysis, cell subcluster analysis, pathway enrichment analysis, spatial mapping of genes and pathways, aging gene analysis, and LARIS spatial interaction analysis, to delineate the high-resolution spatial transcriptomic landscape of dental pulp aging. Our findings provide the first high-resolution spatial molecular atlas of dental pulp aging, offering an exploratory and comprehensive spatial molecular basis for the rational design of novel interventional strategies for vital pulp therapy, even pulp regeneration, and clinical endodontic treatment in aged pulp.

RESULTS

Spatial transcriptomic Visium HD analysis of differentially expressed genes in young and aged pulp tissues with histological validation

We performed high-resolution spatial transcriptomic sequencing on three young and three aged dental pulp tissues using the 10× Genomics Visium HD platform, aiming to explore the mechanisms of pulp aging from a spatial transcriptomic perspective. The Visium HD platform conducts high-resolution gene expression analysis on tissue sections within a 6.5 × 6.5 mm square capture area, which contains approximately 11 million densely arranged 2 × 2 μm oligos, each harboring thousands of capture probes that bind to target sequences and carry spatial barcode information. The most commonly used analytical unit, also referred to as a bin, is typically an 8 × 8 μm rectangular

region composed of 16 2 × 2 μm squares, primarily considering factors such as the average cell size in the tissue. Our study is also based on bins of this size (Fig. 1a).

H&E staining images of tissue sections showed the morphology of young and aged pulp tissues. Young pulp tissue appeared more voluminous and loose compared with aged pulp tissue, whereas aged pulp tissue was thinner, denser, and exhibited a fibrotic tendency (Fig. 1b). To further validate the reliability of the spatial transcriptomic sequencing data, we performed immunofluorescence staining for four downregulated differentially expressed genes—*SELENOP*, *MMP-9*, *MMP-2*, and *TGF-β1*—on human young and aged pulp tissue sections and compared them with the spatial transcriptomic results. IF staining of consecutive sections revealed that the expression of *SELENOP*, *MMP-9*, *MMP-2*, and *TGF-β1* was markedly downregulated in aged pulp tissue compared with young pulp tissue (Fig. 1d, f, h, j), which was consistent with the spatial transcriptomic analysis results (Fig. 1e, g, i, k).

The volcano plot showed that in aged pulp tissue, genes such as *PAEP*, *PTGDS* (which catalyzes the production of prostaglandin D2 (PGD2) and participates in inflammation and immunity processes[15]), and *FOSB* (which forms the transcription factor AP-1 and broadly regulates important physiological processes such as cell proliferation, survival, and apoptosis[16,17]) were significantly upregulated, whereas genes such as *SERPINA3* (studies have shown it can promote tissue repair and regeneration[18–20]), *NNMT* (studies have demonstrated that *NNMT* is associated with cellular senescence; its expression is significantly downregulated in various senescent cell models and is closely linked to the senescence phenotype[21,22]), *CEBPB* (studies have indicated its important role in cell differentiation, immune inflammation, metabolism, aging, and tumorigenesis[23,24]), and *MMP-9* (which participates in extracellular matrix degradation in normal physiological processes, such as embryonic development, reproduction, and tissue remodeling, etc.[25]) were significantly downregulated (Fig. 1c).

Violin plots showed the expression of the upregulated *PTGDS* gene (Fig. S1A) and the downregulated *DIO2* gene (studies have shown that it promotes osteogenic/odontogenic differentiation in human stem cells from the apical papilla (SCAPs)[26]) (Fig. S1C) in pulp tissues. Spatial mapping also showed upregulation of *PTGDS* (Fig. S1B) and downregulation of *DIO2* (Fig. S1D) in aged pulp tissues. GO enrichment analysis indicated that the differentially expressed genes in aged pulp were significantly associated with inflammation-related pathways such as the inflammatory response pathway, tissue regeneration-related pathways such as vasculature development, respiratory burst, and regeneration, and aging-related pathways such as response to alcohol and response to hyperoxia (Fig. S1E). KEGG enrichment analysis suggested that the differentially expressed genes in aged pulp were significantly associated with signaling pathways such as the PI3K-Akt signaling pathway, MAPK signaling pathway, FoxO signaling pathway, and p53 signaling pathway (Fig. S1F).

These results may suggest that, at the transcriptomic level, aged pulp generally shifts toward a

pro-inflammatory and pro-fibrotic state, whereas programs related to tissue mineralization, angiogenesis, and regeneration are broadly suppressed; aging-related signaling pathways such as PI3K-Akt and MAPK may synergistically drive this degenerative process.

Spatial transcriptomic Visium HD identified eight cell populations in young and aged dental pulp tissues

Based on known marker genes[27–35] and spatial location information, we identified eight major cell types in young and aged dental pulp: fibroblasts, progenitor cells, endothelial cells, neural cells, plasma cells, T cells, monocytes, and macrophages. Violin plots showed the expression of the respective marker genes *COL1A2*, *NES*, *VWF*, *MPZ*, *IGKC*, *TRBC2*, *LYZ*, and *CD68* for fibroblasts, progenitor cells, endothelial cells, neural cells, plasma cells, T cells, monocytes, and macrophages (Fig. 2a). Spatial transcriptomic maps displayed the distribution and proportion of cells in young and aged pulp tissues, which were consistent with the anatomical structure of the pulp tissue and visualized at 8 × 8 μm bin resolution. In young pulp tissue, progenitor cells were predominantly located at the periphery of the tissue section and also distributed around the vascular endothelium, whereas in aged pulp tissue, the proportion and number of progenitor cells were significantly reduced compared with young pulp, and they were mainly distributed around the vascular endothelium, with a marked reduction of progenitor cells at the periphery of the tissue section; fibroblasts, as the main component of the pulp tissue, were widely distributed throughout the tissue; endothelial cells, neural cells, and immune cells were diffusely and evenly distributed in the pulp tissue, but immune cells in aged pulp tissue were reduced compared with young pulp tissue (Fig. 2b). UMAP demonstrated that the marker genes *COL1A2*, *NES*, *VWF*, *MPZ*, *IGKC*, *TRBC2*, *LYZ*, and *CD68* corresponded to the spatial clustering distribution of fibroblasts, progenitor cells, endothelial cells, neural cells, plasma cells, T cells, monocytes, and macrophages (Fig. 2c). The spatial transcriptomic maps further validated the spatial correspondence between these marker genes and each cell population (Fig. 2d).

Spatial landscape of fibroblasts

The volcano plot showed that, compared with fibroblasts from young pulp tissue, genes such as *SERPINA3* and *DEPP1* (which has been shown to play an important role in maintaining chondrocyte viability[36] and regulating stem cell differentiation[37,38]) were significantly downregulated, whereas *PTGDS*, etc., were significantly upregulated in fibroblasts from aged pulp tissue (Fig. 3a). GO enrichment analysis indicated that the differentially expressed genes between

fibroblasts from aged and young pulp tissues were significantly associated with inflammation-related pathways such as inflammatory response; tissue regeneration-related pathways such as cell activation, regulation of hemopoiesis, biomineral tissue development and vasculature development; and oxidative stress-related pathways such as regulation of response to oxidative stress (Fig. 3b). Violin plots and spatial co-expression maps showed that both the biomineral tissue development and regulation of hemopoiesis pathways were downregulated in aged pulp fibroblasts (Fig. 3c, d).

UMAP of fibroblast subcluster analysis in young and aged pulp performed using the Seurat package showed that fibroblasts were divided into 16 subclusters (Fig. 3e). The dot plot displayed the expression of some marker genes in each subcluster (Fig. 3f), and subcluster 1, which highly expressed *SERPINA3* and *DEPP1*, showed a markedly reduced proportion in aged pulp (Fig. 3g). Further GO enrichment analysis of all marker genes of fibroblast subcluster 1 indicated that subcluster 1 was significantly associated with GO terms such as extracellular exosome, apoptotic process, and inflammatory response (Fig. 3h).

These results may suggest that a fibroblast subcluster characterized by high expression of *SERPINA3* and *DEPP1*, which is involved in repair and mineralization regulation, is significantly reduced in aged pulp, and the loss of this subcluster may represent an important cellular basis for the aggravated fibrosis and diminished regenerative capacity of aged pulp.

Spatial landscape of progenitor cells

Differential gene analysis showed that, compared with progenitor cells from young pulp tissue, genes such as *SERPINA3*, *IGFBP3* (which has been associated with cellular senescence[39], and reported to be a negative regulator of dental pulp stem cell differentiation[40]), and *FAM20A* (which is essential for amelogenesis and whose loss-of-function mutations cause enamel renal syndrome[41,42]) were significantly downregulated in progenitor cells from aged pulp tissue, whereas genes such as *PTGDS*, *TPM1* (which functions in stabilizing the actin cytoskeleton and regulating muscle contraction, and its deletion promotes hemogenic endothelium (HE) specification and hematopoietic progenitor cell (HPC) generation[43]), and *COCH* (which is preferentially expressed at high levels in the inner ear (cochlea and vestibule), is an important component of the extracellular matrix, and its mutations cause various types of sensorineural deafness[44]) were significantly upregulated (Fig. 4a). GO enrichment analysis of the differentially expressed genes in progenitor cells from aged pulp compared with those from young pulp indicated that these DEGs were significantly enriched in pathways associated with cell proliferation and differentiation, programmed cell death, and tissue regeneration, such as negative regulation of cell population proliferation, positive regulation of programmed cell death, regulation of osteoblast differentiation, biomineral tissue development, collagen metabolic process, regulation of fibroblast proliferation,

and odontogenesis (Fig. 4b). Violin plots of the overall expression of pathway genes and spatial co-expression maps of pathway genes with marker genes both showed that the regulation of fibroblast proliferation and odontogenesis pathways were downregulated in progenitor cells of aged pulp tissue (Fig. 4c, d).

Cell subcluster analysis UMAP showed that progenitor cells in young and aged pulp were divided into 4 subclusters (Fig. 4e). Subcluster 0 highly expressed genes such as *COL21A1* and *CA2*, subcluster 1 highly expressed genes such as *SERPINA3* and *SOCS3* (a key negative regulator of the JAK/STAT signaling pathway. As a negative feedback regulator of cytokine signaling, it can be rapidly induced by the activated JAK/STAT pathway and in turn inhibits this pathway, preventing excessive signal activation[45]), subcluster 2 highly expressed genes such as *GPC3* and *ST8SIA1*, and subcluster 3 highly expressed genes such as *IGKC* and *PHF5A* (Fig. 4f). Compared with young pulp tissue, the proportion of progenitor cell subcluster 1 was significantly reduced in aged pulp tissue (Fig. 4g). GO enrichment analysis of the marker genes of progenitor cell subcluster 1 showed that it was significantly associated with GO terms such as extracellular exosome, nucleolus, mitochondrion, protein folding, and apoptotic process (Fig. 4h).

These analytical results may indicate that the proliferation, odontogenic/odontoblastic differentiation, and collagen metabolic capacity of pulp progenitor cells decline comprehensively with aging; the marked loss of subcluster 1 may compromise the functions of maintaining pulp homeostasis and mineralized repair.

Spatial landscape of endothelial cells

Differential gene analysis showed that in endothelial cells of aged pulp, genes such as *ADAMTS9* (which coordinates tissue remodeling during development[46,47] and exerts anti-angiogenic effects[48]) and *NNMT* were significantly downregulated, whereas genes such as *FOS* (studies suggest that it may play a complex and sometimes dual role in cellular senescence[49]) and *JUN* (which can form homodimers with itself or heterodimers with *FOS* to constitute the important eukaryotic transcription factor AP-1, broadly regulating essential physiological processes such as cell proliferation, survival, and apoptosis[16,17]) were significantly upregulated (Fig. 5a). GO enrichment analysis indicated that the differentially expressed genes in endothelial cells from young and aged pulp were mainly enriched in pathways related to tissue (especially vascular tissue) regeneration and development, such as blood vessel development, regulation of vasculature development, cell activation, response to growth factor, connective tissue development, etc. (Fig. 5b). Violin plots of gene expression and spatial co-expression maps showed that the blood vessel development and connective tissue development pathways were downregulated in endothelial cells of aged pulp (Fig. 5c, d).

Cell subcluster analysis UMAP showed that endothelial cells in young and aged pulp were divided into 3 subclusters (Fig. 5e). Subcluster 0 highly expressed genes such as *CCL14* and *DNASE1L3*; subcluster 1 highly expressed genes such as *ACTG2* (a key gene for maintaining visceral smooth muscle function[50]); subcluster 2 highly expressed genes such as *MPZ* and *SLC10A4* (Fig. 5f). Spatial transcriptomic maps showed that the proportion of endothelial cell subcluster 1 was markedly reduced in aged pulp tissue (Fig. 5g). GO enrichment analysis of the marker genes of subcluster 1 showed that it was significantly associated with GO terms such as extracellular exosome, protein transport, angiogenesis, cell migration, and negative regulation of apoptotic process (Fig. 5h).

These results may indicate that an endothelial cell subcluster with active angiogenic and cell migration capabilities is significantly reduced in aged pulp, accompanied by the downregulation of *ADAMTS9*, which may be associated with the decline in the neovascularization and maintenance capacity of the pulp microvasculature, as well as the diminished nutrient supply and repair function in aged pulp.

Spatial landscape of neural cells

The volcano plot showed that in neural cells of aged pulp, genes such as *ABRAXAS1* (which encodes the protein Abraxas 1, a core scaffold protein of the BRCA1-A complex that plays a key role in DNA damage repair and maintenance of genomic stability[51,52]) and *SERPINA3* were significantly downregulated, whereas genes such as *IGHG3* (which encodes the heavy chain constant region of immunoglobulin G3 (IgG3) and plays a critical role in humoral immune responses[53]) and *FOS* were significantly upregulated (Fig. 6a). We performed GO enrichment analysis on the differentially expressed genes in neural cells from aged pulp relative to those from young pulp, and the results showed that the DEGs were significantly enriched in aging- and inflammation-related pathways, such as DNA-binding transcription factor binding, negative regulation of cell cycle, blood microparticle, inflammatory response, and chromatin binding (Fig. 6b). Violin plots of gene expression and spatial co-expression maps showed that the DNA-binding transcription factor binding pathway was upregulated in aged pulp neural cells (Fig. 6c), whereas the blood microparticle pathway was downregulated in aged pulp neural cells (Fig. 6d).

Cell subcluster analysis results showed that neural cells in young and aged pulp were divided into 2 subclusters (Fig. 6e). Subcluster 0 highly expressed genes such as *ERBB3* and *UTRN*, and subcluster 1 highly expressed genes such as *AHNAK* (which encodes a giant scaffold protein that plays a central role in cell membrane repair, calcium signaling regulation, cytoskeletal organization, and signal transduction[54]) and *DENND2A* (Fig. 6f). Spatial transcriptomic map visualization showed that the distribution and proportion of neural cells were similar between young and aged

pulp tissues, and subcluster 1 exhibited a slightly greater magnitude of change than subcluster 0, with its proportion slightly increased in aged pulp tissue (Fig. 6g). Furthermore, we performed GO enrichment analysis on the marker genes of subcluster 1, and the results showed that the enriched GO terms of its marker genes included response to endoplasmic reticulum stress, autophagosome maturation, rhythmic process, and mitochondrial calcium ion homeostasis (Fig. 6h).

These results may suggest that although the number of neural cells in aged pulp does not change substantially, they still undergo a series of aging-related changes, such as the downregulation of the DNA damage repair gene *ABRAXAS1* and a mild expansion of subcluster 1, reflecting adaptive responses to endoplasmic reticulum stress and mitochondrial calcium homeostasis imbalance.

Spatial landscape of immune cells

Differential gene analysis showed that, compared with immune cells from young pulp, genes such as *GPX3* (which plays a critical role in defending against oxidative stress[55]), *CD74* (which functions as a molecular chaperone to assist immune responses[56]), *IFI6* (which exerts antiviral, anti-apoptotic, and other effects[57,58]), and *FOS* were significantly downregulated in immune cells from aged pulp, whereas genes such as *ANKRD10*, *GEMIN4*, and *MAP2K4* (which can broadly participate in regulating apoptosis, inflammation, cell motility, development, and immune homeostasis by activating pathways such as MAPK[59,60]) were significantly upregulated (Fig. 7a). GO enrichment analysis of the differentially expressed genes in immune cells from the two pulp groups revealed that pathways such as response to steroid hormone, response to oxidative stress, response to growth factor, negative regulation of cell motility, response to metal ion, and MAPK cascade were enriched (Fig. 7b). Violin plots and spatial co-expression maps showed that the response to growth factor and MAPK cascade pathways were downregulated in aged pulp (Fig. 7c, d).

Spatial transcriptomic maps showed that in aged pulp tissue, the proportion of plasma cells was upregulated, the proportions of monocytes and macrophages were downregulated, and the proportion of T cells remained essentially unchanged (Fig. 7e). In the GO enrichment analysis described above, FOS was among the genes contributing to all six displayed pathways (highlighted in the figure) (Fig. 7b). Therefore, we further mapped the *FOS* gene onto young and aged pulp tissues (Fig. 7f), and the gene expression violin plots also showed that *FOS* was downregulated in all four types of immune cells in aged pulp, most prominently in monocytes (Fig. 7g).

These results may suggest that pulp aging is accompanied by remodeling of the immune cell composition, with a decrease in monocytes/macrophages and a relative increase in plasma cells, along with the downregulation of antioxidant defense, growth factor response, and MAPK signaling. This may weaken innate and reparative immune functions, creating an immune microenvironment

that favors chronic inflammation and impaired regeneration.

Aging-related gene analysis

To further investigate changes in aging-related genes in aged pulp tissue, we performed intersection analysis between the 272 differentially expressed genes in aged versus young pulp and the 503 aging-related genes obtained from the Aging Atlas website[61]. Of the 272 DEGs and 503 aging-related genes, 14 overlapped (Fig. 8a); among these, 5 were upregulated and 9 downregulated in aged pulp tissue (Fig. 8b). Volcano plots and bubble plots displayed the expression of the differentially expressed genes and the overlapping genes. The results showed that aging-related genes such as *CXCL8*, *PPARG*, *NGFR*, *FLT1*, and *S100B* were significantly upregulated in aged pulp tissue, whereas aging-related genes such as *SOD2*, *CEBPB*, *RELB*, *CD14*, *C1QA*, *IGFBP3*, *TNFAIP3*, *STAT3*, and *PLAUR* were significantly downregulated (Fig. 8c, d). Violin plot analysis confirmed that *IGFBP3* was significantly downregulated in aged pulp tissue (Fig. 8e). Spatial mapping showed that *IGFBP3* expression largely overlapped with the distribution of progenitor cells in both young and aged pulp (Fig. 8f, g). Further analysis of *IGFBP3* gene expression in different cells also indicated that it was significantly downregulated in progenitor cells of aged pulp (Fig. 8h), suggesting that the *IGFBP3* gene may play an important role in pulp aging by affecting progenitor cells.

We further performed GO and KEGG enrichment analysis on the obtained aging-related differentially expressed genes, and the results showed that these genes were significantly enriched in GO pathways such as negative regulation of cell population proliferation, inflammatory response, regulation of apoptotic signaling pathway, positive regulation of apoptotic process, regulation of angiogenesis, regulation of endothelial cell proliferation, astrocyte differentiation, and response to hypoxia (Fig. S2A), as well as significantly enriched in KEGG pathways such as transcriptional misregulation in cancer, NF-kappa B signaling pathway, MAPK signaling pathway, IL-17 signaling pathway, necroptosis, longevity regulating pathway, growth hormone synthesis/secretion and action, and cellular senescence (Fig. S2B).

These results may suggest that pulp aging is not driven by a single aging gene but rather manifests as transcriptional dysregulation characterized by the downregulation of protective genes such as *SOD2*[62–64] and *TNFAIP3*[65,66] and the upregulation of pro-inflammatory/pro-apoptotic genes such as *CXCL8*[67–69] and *NGFR*[70]. This imbalance may synergistically exacerbate oxidative stress, inflammation, and apoptotic pressure within the tissue through signaling pathways such as NF-κB, MAPK, and cellular senescence, thereby driving the pulp toward irreversible degenerative changes.

Cell–cell interaction analysis

We performed cell–cell interaction analysis specifically designed for spatial transcriptomic sequencing data (LARIS spatial interaction analysis)[71] on young and aged pulp tissues. In young pulp, bidirectional *MPZ–MPZ* interactions (highlighted in blue) were detected between neural cells and fibroblasts, between neural cells and neural cells, and between neural cells and plasma cells. In aged pulp, only *MPZ–MPZ* interactions between neural cells remained detectable. *PTN–SDC3* interactions were markedly increased in aged pulp compared with young pulp (highlighted in green); in young pulp, these interactions mainly occurred between fibroblasts, plasma cells, and monocytes and progenitor cells, whereas in aged pulp, monocytes, macrophages, and other cells engaged in extensive bidirectional *PTN–SDC3* interactions with other cells. In young pulp, fibroblasts and immune cells engaged in extensive *COL1A2–CD44* interactions with fibroblasts, plasma cells, T cells, and macrophages, whereas in aged pulp, only unidirectional *COL1A2–CD44* interactions were observed between progenitor cells, plasma cells, macrophages, and macrophages (highlighted in red) (Fig. 9a).

The heatmap of the number of cell–cell interactions also showed that, compared with the extensive intercellular interactions in young pulp, the interactions in aged pulp tissue were attenuated and mainly concentrated among neural cells and monocytes (Fig. 9b, c). Further difference analysis of cell–cell interaction scores between young and aged pulp also indicated that neural cell–neural cell and monocyte–monocyte interaction scores exhibited the greatest changes in aged pulp, with neural cell–neural cell interactions markedly weakened and monocyte–monocyte interactions markedly enhanced in aged pulp (Fig. 9d).

We performed spatial visualization of the *MPZ–MPZ* interaction pair, which exhibited notable changes and involved neural cell–neural cell interactions, in young and aged pulp. The results showed that in young pulp, *MPZ*-expressing neural cells, fibroblasts, and plasma cells were in close spatial proximity, whereas in aged pulp, these three cell types were diffusely distributed (Fig. 9e, f). These results further validated that *MPZ–MPZ*-based interactions could occur bidirectionally between neural cells and between neural cells and plasma cells in young pulp tissue, whereas in aged pulp, only neural cell–neural cell interactions were present, and the *MPZ–MPZ* interactions between neural cells were attenuated compared with young pulp. These results may suggest that the decline in innervation capacity in aged pulp may be associated with a reduced range of intercellular communication of neural signals.

DISCUSSION

This study is the first to systematically apply high-resolution spatial transcriptomics (Visium HD, 8 × 8 μm bin resolution) to the study of human pulp aging. Compared with traditional bulk RNA-seq and single-cell RNA-seq, this technology not only preserves in situ spatial information of the tissue but also overcomes the bottleneck of spatial signal loss inherent in cell suspension preparations. We found that pulp aging is not a homogeneous process but exhibits pronounced regional heterogeneity—for example, progenitor cells are enriched at the periphery and around blood vessels in young pulp, whereas after aging, their distribution is nearly restricted to the perivascular area, suggesting that the local microenvironment (e.g., oxygen gradient, extracellular matrix stiffness) may play a critical role in progenitor cell survival. This novel spatial insight provides reference evidence for understanding regional degeneration of the pulp (e.g., earlier aging in the apical region than in the coronal region).

Only three samples were included per group in this study, mainly due to the considerable difficulty in obtaining healthy young and aged human pulp specimens and the stringent sample quality requirements for transcriptomic sequencing (a strict quality control criterion of DV200 > 30%). Nevertheless, we independently validated four key proteins (*MMP-9*, *TGF-β1*, *SELENOP*, *MMP-2*) on consecutive sections using multiplex immunofluorescence (TSA technology), and the expression trends were highly consistent with the spatial transcriptomic data, indicating that the current results possess high internal consistency and biological reproducibility. As an exploratory foundational study, the current work provides robust hypotheses for subsequent large-scale validation.

In this study, we observed an intriguing phenomenon: three cell types of entirely distinct lineages—fibroblasts, progenitor cells, and endothelial cells—each exhibited a marked reduction in a specific subcluster during aging, and these subclusters were all significantly enriched in the "extracellular exosome" pathway. Specifically, the fibroblast subcluster expressing *SERPINA3*/*DEPP1*, the progenitor cell subcluster expressing *SERPINA3*/*SOCS3*, and the endothelial cell subcluster expressing *ACTG2*/*PLN* were all markedly reduced in aged pulp. These results may suggest that, during pulp aging, the core functions of different cell types are compromised, and that these sensitive subclusters may undergo functional changes through the exosome pathway, potentially co-constructing a cross-lineage "aging exosome network." We hypothesize that under aging stress, the impairment of these sensitive subclusters may lead them to release exosomes carrying pro-inflammatory or aberrant regulatory signals, which interact within the microenvironment to synergistically amplify local inflammatory and fibrotic signals, ultimately contributing to tissue-wide homeostatic collapse.

Compared with fibroblasts, progenitor cells, and endothelial cells, neural cells in the pulp exhibited the least differential changes during aging. However, further cell–cell interaction analysis revealed that neural cells play a pivotal role in constructing the interaction networks in both young and aged pulp, and that *MPZ–MPZ* interactions among neural cells themselves were markedly

weakened in aged pulp, while *MPZ–MPZ* interactions between neural cells and other cell types disappeared. These results may suggest that even subtle dysfunction of neural cells in the pulp can promote the pulp aging process, and also remind us to emphasize neural cell function in future pulp regeneration and anti-aging strategies.

CXCL8 (also known as *IL-8*) is a key molecule of the senescence-associated secretory phenotype (SASP), regulated by pathways including NF-kappa B, and its expression is upregulated in aged tissues and cells[67–69], participating in and potentially exacerbating aging and related inflammatory processes in tissues including the dental pulp and periodontium[72–74]. Previous studies have shown that *CXCL8* in the dental pulp is mainly regulated by the visfatin/TLR4 signaling axis to participate in the aging process[72]. In our study, aging-related gene enrichment analysis showed that *CXCL8*, which was upregulated in aged pulp, participated in the GO pathways negative regulation of cell population proliferation and inflammatory response (Fig. S2A), as well as the KEGG pathways NF-kappa B signaling pathway and IL-17 signaling pathway ((Fig. S2B). These results are partially consistent with previous studies and further suggest other pathways and roles that *CXCL8* may involve in and exert in pulp aging.

The changes in *IGFBP3* in senescent cells and its specific roles and mechanisms in aging remain incompletely understood and inconsistent across studies. One study on human dermal fibroblasts reported that *IGFBP3* expression was significantly upregulated in senescent human dermal fibroblasts; although *IGFBP3* has a pro-apoptotic function, in senescent human dermal fibroblasts it was not endocytosed into the nucleus to exert pro-apoptotic effects but instead functioned in the cytoplasm and extracellular space to "block growth factor signaling and consolidate the senescent state," thereby exerting a pro-aging effect[75]. In contrast, another study on human lung fibroblast senescence found that *IGFBP3* expression was significantly lower in senescent human lung fibroblasts and H_2O_2-induced senescent human lung fibroblasts compared with young cells, speculating that *IGFBP3* may be an anti-aging protective factor and that its reduction leads to overactivation of the PI3K/Akt/mTOR and p53 pathways, ultimately driving the aging process[76]. Its role in pulp aging merits further investigation.

In the cell–cell interaction analysis, we also found that the interaction of the tight junction protein *CLDN11–CLDN11*[77] (highlighted in red box) was widely present only in young pulp tissue, involving bidirectional interactions among fibroblasts, monocytes, and macrophages (Fig. 9a), which may suggest tighter intercellular connections in young pulp and a decrease in cell junction integrity due to aging. Meanwhile, the adhesion-related interaction molecules *PECAM1–PECAM1*[78] and *ESAM–ESAM*[79] (highlighted in green box) were specifically present in endothelial cells of aged pulp (Fig. 9a), suggesting that aging leads to altered vascular endothelial barrier function, which may be associated with increased vascular permeability and decreased blood supply in aged pulp.

In summary, we constructed a high-resolution spatial transcriptomic atlas of human pulp aging using the Visium HD platform for the first time, systematically revealing cell-type-specific

alterations and spatial microenvironment changes during aging. At the molecular level, aged pulp exhibited a shift toward a pro-inflammatory and pro-fibrotic state, while programs associated with mineralization, angiogenesis, and tissue regeneration were broadly suppressed; signaling pathways such as PI3K-Akt, MAPK, and FoxO may serve as potential core drivers. The fibroblast subcluster (highly expressing *SERPINA3*/*DEPP1*) was significantly reduced in aged pulp, along with corresponding decreases in a progenitor cell subcluster (highly expressing *SERPINA3*/*SOCS3*) and an endothelial cell subcluster (highly expressing *ACTG2*/*PLN*)—all of these subclusters showed enrichment of extracellular exosome and apoptosis-related pathways, suggesting a possible common aging-associated phenotype. Neural cells exhibited a mild stress response. The immune microenvironment of aged pulp underwent pro-inflammatory remodeling, manifested by a decrease in monocytes/macrophages and an increase in plasma cells, together with diminished antioxidant defense and growth factor responsiveness. Intersection analysis of aging-related genes further indicated that pulp aging is not driven by a single aging gene but rather by transcriptional dysregulation of genes such as *SOD2*, *TNFAIP3*, *CXCL8*, and *NGFR*; this dysregulation may promote irreversible degenerative changes in the pulp through signaling pathways including NF-κB, MAPK, and cellular senescence. Furthermore, LARIS spatial interaction analysis revealed significantly attenuated intercellular communication in aged pulp, with a markedly narrowed scope of *MPZ–MPZ* interactions between neural cells and altered *PTN–SDC3* and *COL1A2–CD44* interaction patterns. The spatial molecular changes identified in this study, particularly the reduction of specific functional subclusters, the enhancement of pro-inflammatory signals, and the alterations in cell–cell interaction patterns in aged pulp tissues, provide an innovative theoretical basis and potential intervention targets for vital pulp therapy and subcluster-targeted regenerative strategies in aged pulp.

MATERIALS AND METHODS

Tissue acquisition

Pulp tissues examined in this work were sourced from non-functional third molars or healthy teeth extracted for orthodontic purposes. Individuals with systemic diseases were excluded. All samples possessed intact structures, with no caries or enamel demineralization evident. Donors reported no painful or uncomfortable symptoms, and histological assessment verified the healthy status of the pulp. Radiographic examinations revealed no abnormalities. Table S1 lists comprehensive donor and sample details. Following extraction, teeth were promptly disinfected and sectioned to expose the pulp, which was then preserved in fixative for downstream experiments.

All experimental protocols were approved by the Medical Ethics Committee of the Hospital of Stomatology, Sun Yat-sen University (approval KQEC-2025-081-01). All methods were

carried out in accordance with institutional guidelines and the Declaration of Helsinki. Written informed consent was obtained from all donors prior to sample collection.

Formalin-fixed paraffin-embedded (FFPE) section preparation

Aseptically isolated pulp tissues were fixed in 4% paraformaldehyde for 12–24 hours. A stepwise dehydration process was applied using ethanol baths of ascending concentrations (30%, 50%, and 70%, each for 45–60 minutes), followed by an overnight incubation in 75% ethanol, and then further treatment with 80%, 95%, and 100% ethanol (45–60 minutes per step). After dehydration, samples were cleared in xylene to displace ethanol, infiltrated with low-melting-point paraffin to replace xylene, and embedded in molten paraffin that was rapidly cooled on a pre-chilled surface. Finally, a microtome was employed to cut sections at a thickness of 5 μm for spatial transcriptomics and 5 μm for immunofluorescence.

Visium HD spatial gene expression

Total RNA was extracted from FFPE blocks using the RNeasy FFPE Kit (73504, Qiagen), and its integrity was evaluated via the DV200 metric. Only sections with DV200 > 30% proceeded to the spatial transcriptomics assay (all samples in this study had DV200 $\geqslant$ 40%). The Visium HD protocol employs dedicated slides that must be thawed, rinsed, and equilibrated in designated buffers; these slides incorporate high-resolution fiducial markers for subpixel-level image registration and include a dispensing pad with a spacer to facilitate CytAssist operation. In accordance with the Visium HD FFPE Tissue Preparation Handbook (CG000684), FFPE sections were first placed on standard glass slides, deparaffinized, subjected to H&E staining, and scanned under brightfield illumination at 20× magnification with a PANNORAMIC MIDI II Digital Scanner (3DHISTECH). Subsequent steps—probe hybridization, ligation, slide processing, probe release, extension, library preparation, and sequencing—were executed as directed by the Visium HD Spatial Gene Expression Reagent Kits User Guide (CG000685). Sequencing was performed on a NovaSeq 6000 system (Illumina) generating paired-end reads (Read 1: 43 cycles; i7: 10 cycles; i5: 10 cycles; Read 2: 50 cycles). Space Ranger (v3.0.0) was used to align FASTQ data to the human genome, detect tissue areas, co-register sequencing information with microscope and CytAssist images, and construct gene-barcode count matrices.

Clustering and cell type annotation

For each dental pulp (DP) specimen, a Seurat object (v5.2.0) was initiated from the 8 × 8 μm filtered feature-barcode matrix. Bins with fewer than 100 UMI or fewer than 50 detected genes were eliminated. Raw counts were log-normalized, and preliminary clustering was performed within Seurat at a resolution of 0.3. To account for the possibility that individual spatial bins may contain

captures from more than one cell, DoubletFinder (v2.0.4) was applied to identify and remove bins with expression profiles suggestive of mixed cell populations. After discarding low-quality bins and putative doublets, data were re-normalized with NormalizeData, highly variable features were selected using FindVariableFeatures, and expression values were scaled with ScaleData. PCA was computed with RunPCA for dimensionality reduction, and graph-based clustering was carried out by FindNeighbors and FindClusters. The results were displayed with DimPlot.

Marker genes for each cluster were found using FindAllMarkers, followed by enrichment analysis with the clusterProfiler package (v4.12.6) on default settings, referencing human gene annotations from org.Hs.eg.db. Cell type identities were assigned based on known marker genes and spatial location information.

Spatial visualization

For spatial visualization, bin clustering and UMAP[80] projections were generated using Space Ranger (v3.0.0) and subsequently imported into Loupe Browser (v8.1.1, 10× Genomics). In this workflow, Space Ranger performs normalization, PCA-based dimensionality reduction, and graph-based clustering, and the resulting clusters together with the UMAP coordinates were directly visualized and further customized within the Loupe Browser interface.

GO/KEGG enrichment analysis

Differential gene expression testing was conducted in Seurat through the FindMarkers function applying the bimod likelihood-ratio test. Genes were considered significantly altered if $|\log_2$ fold change$| > 0.5$ and adjusted *P*-value (Benjamini–Hochberg) < 0.05, and these DEGs were illustrated by a volcano plot. Filtered DEGs were submitted to Metascape (http://metascape.org) for GO and KEGG pathway enrichment, employing a *P*-value cutoff of 0.05. GO/KEGG terms with q-values less than 0.05 were depicted on the CNSknowall platform (https://cnsknowall.com). Finally, the spatial patterns of the significantly enriched pathways were projected onto the dental pulp sections within Loupe Browser (10× Genomics).

Immunofluorescence staining and multispectral imaging

Multiplex immunofluorescence staining was performed on 5 μm formalin-fixed, paraffin-embedded (FFPE) human dental pulp sections using a tyramide signal amplification (TSA)-based four-color five-channel protocol (Servicebio). The specimens comprised three young and three aged donor samples, which were derived from the same cohort as the spatial transcriptomic analysis. Adjacent serial sections were employed to ensure optimal morphological correspondence with the transcriptomic data.

Following deparaffinization in xylene substitutes and rehydration through a graded ethanol series, antigen retrieval was carried out by heating the sections in Tris-EDTA buffer (pH 8.0) for 30 min using an antigen retrieval instrument (ARI-4, Servicebio). Endogenous peroxidase activity was quenched by incubating the sections in 3% H_2O_2–methanol solution for 25 min at room temperature in the dark. Subsequently, non-specific binding sites were blocked with 3% bovine serum albumin (BSA) for 30 min at room temperature.

The sequential TSA-based staining was executed as follows. In the first cycle, sections were incubated overnight at 4 °C with a primary antibody against MMP-9 (mouse monoclonal, Servicebio, #GB120004, 1:3000), followed by incubation with an S-vision polymer HRP goat anti-mouse secondary antibody (Servicebio, #G1301, ready-to-use) for 50 min at room temperature, and finally visualized with iF440-Tyramide (Servicebio, #G1250, 1:100) for 10 min at room temperature. After each cycle, bound antibodies were stripped by applying an antibody stripping solution (Servicebio, #G1266) for 30 min at 37°C. This procedure was repeated for the remaining targets in the following order: TGF-β1 (rabbit monoclonal, Servicebio, #GB15179, 1:10000) detected with S-vision polymer HRP goat anti-rabbit secondary antibody (Servicebio, #G1302, ready-to-use) and iF488-Tyramide (Servicebio, #G1231, 1:500); SELENOP (rabbit polyclonal, Servicebio, #GB114931, 1:8000) detected with the same S-vision polymer HRP goat anti-rabbit secondary antibody and iF546-Tyramide (Servicebio, #G1251, 1:500); and MMP-2 (rabbit polyclonal, Servicebio, #GB11130, 1:10000) detected with iF594-Tyramide (Servicebio, #G1242, 1:500). Extensive washes with PBS or Tris-buffered saline with Tween 20 (TBST) were performed between all steps. Antibody information is provided in Table S2.

Following the four TSA cycles, nuclei were counterstained with DAPI (Servicebio, #G1012) for 10 min at room temperature. To minimize tissue autofluorescence, sections were incubated with an autofluorescence quencher (Servicebio, #G1221) for 5 min, after which the slides were mounted with an anti-fade mounting medium (Servicebio, #G1401). Whole-slide images were acquired using a digital slide scanning system (Pannoramic MIDI, 3DHISTECH).

Image analysis and quantification

Quantitative evaluation of the immunofluorescence signals was carried out using the digital pathology software Saiviewer-2.3.1 (Servicebio). For each target protein (MMP-9, TGF-β1, SELENOP, and MMP-2), the relative expression level was assessed using the positive number (PN), defined as the ratio of the mean fluorescence intensity of the specific protein signal to that of the DAPI nuclear counterstain within the defined regions of interest. This calculation was performed independently for all three young and three aged dental pulp samples.

Spatial intercellular communication analysis

To investigate spatially restricted intercellular communication, we employed LARIS (v1.0.0). Based on physical coordinates, LARIS constructs a spatial k-nearest neighbors (k-NN) graph and applies gene expression diffusion to calculate high-resolution ligand-receptor (LR) interaction scores. This approach enabled us to identify spatially significant, cell-type-specific signaling networks and sender-receiver communication patterns across the tissue architecture.

Statistical analysis

All statistical analyses were conducted using GraphPad Prism 9.0.0 (GraphPad Software, Inc., San Diego, CA, USA). Data are presented as the mean ± standard deviation (SD). To compare protein expression between the young and aged groups, the PN values for each of the four proteins were analyzed separately using an unpaired, two-tailed Student's *t*-test. A P-value < 0.05 was considered statistically significant. Quantitative results were visualized as bar graphs illustrating the differences in PN values for each protein between the two groups.

DATA AVAILABILITY

Data supporting this study are available from the corresponding author upon reasonable request.

ACKNOWLEDGEMENTS

This work was financial supported by the Guangdong Basic and Applied Basic Research Foundation (No.2022A1515011266, No.2022A1515110601), National Natural Science Foundation of China (No.81700950, No.82370943). We are grateful for bioinformatics support from Bailin Duan (LC-Bio Technology co., ltd.)

AUTHOR CONTRIBUTION

Fengyuan Zhang: investigation, methodology, visualization, writing – original draft preparation, writing – review & editing. Yuanyuan Kong: investigation, methodology, visualization, writing – original draft preparation, writing – review & editing. Jiayi Wang: investigation, methodology, visualization, writing – original draft preparation, writing – review & editing. Manlin Xu: investigation, methodology, visualization, writing – original draft preparation. Xiaobin Fu: investigation, methodology, visualization. Jiyuan Zuo: investigation, methodology, visualization. Qining Guo: investigation, methodology, visualization. Qianzhou Jiang: supervision. Junqi Ling: funding acquisition, project administration, supervision. Jianmao Zheng: funding acquisition, project administration, supervision.

ADDITIONAL INFORMATION

Supplementary information

Supplementary information accompanies the manuscript on the *International Journal of Oral Science* website (http://www.nature.com/ijos).

Competing interests

The authors declare no competing interests.

Ethics approval

This study was approved by the Medical Ethics Committee of the Hospital of Stomatology, Sun Yat-sen University (approval KQEC-2025-081-01). All methods were carried out in accordance with institutional guidelines and the Declaration of Helsinki. Written informed consent was obtained from all donors prior to sample collection.

References:

1. Galler, K. M., Weber, M., Korkmaz, Y., Widbiller, M. & Feuerer, M. Inflammatory response mechanisms of the dentine–pulp complex and the periapical tissues. *International Journal of Molecular Sciences* **22**, 1480 (2021).
2. Cooper, P. R., Holder, M. J. & Smith, A. J. Inflammation and regeneration in the dentin-pulp complex: A double-edged sword. *J Endod* **40**, S46-51 (2014).
3. Harper, S. Economic and social implications of aging societies. *Science* **346**, 587–591 (2014).
4. de Farias, J. O. & Rezende, T. M. B. Dental pulp and apical papilla cells senescence: Causes, consequences, and prevention. *Biogerontology* **24**, 533–539 (2023).
5. Sun, H. *et al.* Vascular and lymphatic heterogeneity and age-related variations of dental pulps. *J Dent* **138**, 104695 (2023).
6. Moretto, C., Kopper, P. M. P., Münchow, E. A. & Scarparo, R. K. Association between patient age and vital pulp therapy outcomes: A systematic review and meta-analysis of prognostic studies. *Int Endod J* **58**, 809–832 (2025).
7. Chaniotis, A., Sousa Dias, H. & Chanioti, A. Negotiation of calcified canals. *J Clin Med* **13**, 2703 (2024).
8. Tranasi, M. *et al.* Microarray evaluation of age-related changes in human dental pulp. *J Endod* **35**, 1211–1217 (2009).
9. Tong, Z. *et al.* Insulin-like growth factor binding protein 7 identified in aged dental pulp by single-cell RNA sequencing. *J Adv Res* **76**, 371–385 (2025).
10. Yakubovsky, O. *et al.* A spatial atlas of the healthy human liver from live donors. *Nature* **653**, 1148–1157 (2026).
11. Oliveira, M. F. de *et al.* High-definition spatial transcriptomic profiling of immune cell populations in colorectal cancer. *Nat Genet* **57**, 1512–1523 (2025).
12. Zhang, Y. *et al.* Single-cell spatial atlas of smoking-induced changes in human gingival tissues. *Int J Oral Sci* **17**, 60 (2025).
13. Zhang, F. *et al.* Spatial Transcriptomics Delineates the Inflammatory Landscape of Human Dental Pulp: Regional Crosstalk and Therapeutic Implications. *Int Endod J* **59**, 2180–2200 (2026).
14. Rao, A., Barkley, D., França, G. S. & Yanai, I. Exploring tissue architecture using spatial transcriptomics. *Nature* **596**, 211–220 (2021).
15. White, C. A., Ghazan-Shahi, S. & Adams, M. A. β-trace protein: A marker of GFR and other biological pathways. *Am J Kidney Dis* **65**, 131–146 (2015).
16. Abate, C. & Curran, T. Encounters with fos and jun on the road to AP-1. *Semin Cancer Biol* **1**, 19–26 (1990).
17. Rahmsdorf, H. J. Jun: Transcription factor and oncoprotein. *J Mol Med (Berl)* **74**, 725–747 (1996).
18. Wang, L. *et al.* Serpina3k lactylation protects from cardiac ischemia reperfusion injury. *Nat*

Commun **16**, 1012 (2025).
19. Sun, Q. *et al.* Serine protease inhibitor, SerpinA3n, regulates cardiac remodelling after myocardial infarction. *Cardiovasc Res* **120**, 943–953 (2024).
20. de Mezer, M. *et al.* SERPINA3: Stimulator or inhibitor of pathological changes. *Biomedicines* **11**, 156 (2023).
21. Chanvillard, L. *et al.* NNMT inhibition counteracts tubular senescence and fibrosis in early stages of chronic kidney disease. *Cell Rep* **45**, 116823 (2026).
22. Narayanan, A. *et al.* Nicotinamide metabolism reprogramming drives reversible senescence of glioblastoma cells. *Cell Mol Life Sci* **82**, 126 (2025).
23. Niehrs, C. & Calkhoven, C. F. Emerging role of C/EBPβ and epigenetic DNA methylation in ageing. *Trends Genet* **36**, 71–80 (2020).
24. Wang, D. *et al.* Colorectal cancer cell-derived CCL20 recruits regulatory T cells to promote chemoresistance via FOXO1/CEBPB/NF-κB signaling. *J Immunother Cancer* **7**, 215 (2019).
25. Wolosowicz, M., Prokopiuk, S. & Kaminski, T. W. Matrix metalloproteinase-9 (MMP-9) as a therapeutic target: Insights into molecular pathways and clinical applications. *Pharmaceutics* **17**, 1425 (2025).
26. Weng, Y. *et al.* A single-cell transcriptomic atlas of human stem cells from apical papilla during the committed differentiation. *Int Endod J* **58**, 305–321 (2025).
27. Yin, H. *et al.* A dynamic transcriptome map of different tissue microenvironment cells identified during gastric cancer development using single-cell RNA sequencing. *Front Immunol* **12**, 728169 (2021).
28. Robinson, R. S., Hammond, A. J., Mann, G. E. & Hunter, M. G. A novel physiological culture system that mimics luteal angiogenesis. *Reproduction* **135**, 405–413 (2008).
29. Abdel Fattah, A. R. *et al.* Actuation enhances patterning in human neural tube organoids. *Nat Commun* **12**, 3192 (2021).
30. Viña-Almunia, J. *et al.* Influence of different types of pulp treatment during isolation in the obtention of human dental pulp stem cells. *Med Oral Patol Oral Cir Bucal* **21**, e374-379 (2016).
31. Dinh, H. Q. *et al.* Integrated single-cell transcriptome analysis reveals heterogeneity of esophageal squamous cell carcinoma microenvironment. *Nat Commun* **12**, 7335 (2021).
32. Chen, H.-J. *et al.* Meta-analysis of in vitro-differentiated macrophages identifies transcriptomic signatures that classify disease macrophages in vivo. *Front Immunol* **10**, 2887 (2019).
33. Richer, A. L., Riemondy, K. A., Hardie, L. & Hesselberth, J. R. Simultaneous measurement of biochemical phenotypes and gene expression in single cells. *Nucleic Acids Res* **48**, e59 (2020).
34. Wang, Z. *et al.* Single-cell RNA sequencing of peripheral blood mononuclear cells from acute kawasaki disease patients. *Nat Commun* **12**, 5444 (2021).

35. Zhao, J. *et al.* Single-cell RNA sequencing reveals the heterogeneity of liver-resident immune cells in human. *Cell Discov* **6**, 22 (2020).
36. Kuwahara, M. *et al.* C10orf10/DEPP activates mitochondrial autophagy and maintains chondrocyte viability in the pathogenesis of osteoarthritis. *FASEB J* **36**, e22145 (2022).
37. Watanabe, H. *et al.* A novel protein depp, which is induced by progesterone in human endometrial stromal cells activates elk-1 transcription factor. *Mol Hum Reprod* **11**, 471–476 (2005).
38. Chen, S., Gai, J., Wang, Y. & Li, H. FoxO regulates expression of decidual protein induced by progesterone (DEPP) in human endothelial cells. *FEBS Lett* **585**, 1796–1800 (2011).
39. Ushakov, R. E., Aksenov, N. D., Pugovkina, N. A. & Burova, E. B. Effects of IGFBP3 knockdown on human endometrial mesenchymal stromal cells stress-induced senescence. *Biochem Biophys Res Commun* **570**, 143–147 (2021).
40. Zhang, Y., Qiao, W., Ji, Y. & Meng, L. GATA4 inhibits odontoblastic differentiation of dental pulp stem cells through targeting IGFBP3. *Arch Oral Biol* **154**, 105756 (2023).
41. Wang, S.-K. *et al.* FAM20A mutations and transcriptome analyses of dental pulp tissues of enamel renal syndrome. *Int Endod J* **56**, 943–954 (2023).
42. Sriwattanapong, K. *et al.* Deep dental phenotyping and a novel FAM20A variant in patients with amelogenesis imperfecta type IG. *Oral Dis* **30**, 537–550 (2024).
43. Wilken, M. B. *et al.* Tropomyosin 1 deficiency facilitates cell state transitions and enhances hemogenic endothelial cell specification during hematopoiesis. *Stem Cell Reports* **19**, 1264–1276 (2024).
44. Robertson, N. G. *et al.* Inner ear localization of mRNA and protein products of COCH, mutated in the sensorineural deafness and vestibular disorder, DFNA9. *Hum Mol Genet* **10**, 2493–2500 (2001).
45. Stross, C. *et al.* Oncostatin M receptor-mediated signal transduction is negatively regulated by SOCS3 through a receptor tyrosine-independent mechanism. *J Biol Chem* **281**, 8458–8468 (2006).
46. Nandadasa, S., Nelson, C. M. & Apte, S. S. ADAMTS9-mediated extracellular matrix dynamics regulates umbilical cord vascular smooth muscle differentiation and rotation. *Cell Rep* **11**, 1519–1528 (2015).
47. Enomoto, H. *et al.* Cooperation of two ADAMTS metalloproteases in closure of the mouse palate identifies a requirement for versican proteolysis in regulating palatal mesenchyme proliferation. *Development* **137**, 4029–4038 (2010).
48. Lo, P. H. Y. *et al.* Extracellular protease ADAMTS9 suppresses esophageal and nasopharyngeal carcinoma tumor formation by inhibiting angiogenesis. *Cancer Res* **70**, 5567–5576 (2010).
49. Jing, Y. *et al.* Recent research advances of c-fos in regulating cell senescence. *Arch Biochem Biophys* **769**, 110423 (2025).
50. Ceron, R. H. *et al.* Molecular mechanisms linking missense ACTG2 mutations to visceral

myopathy. *Sci Adv* **10**, eadn6615 (2024).
51. Sachsenweger, J. *et al.* ABRAXAS1 orchestrates BRCA1 activities to counter genome destabilizing repair pathways-lessons from breast cancer patients. *Cell Death Dis* **14**, 328 (2023).
52. Wu, X. & Wang, B. Abraxas suppresses DNA end resection and limits break-induced replication by controlling SLX4/MUS81 chromatin loading in response to TOP1 inhibitor-induced DNA damage. *Nat Commun* **12**, 4373 (2021).
53. Kardava, L. *et al.* IgG3 regulates tissue-like memory B cells in HIV-infected individuals. *Nat Immunol* **19**, 1001–1012 (2018).
54. Sundararaj, S., Ravindran, A. & Casarotto, M. G. AHNAK: The quiet giant in calcium homeostasis. *Cell Calcium* **96**, 102403 (2021).
55. Zhang, N., Liao, H., Lin, Z. & Tang, Q. Insights into the role of glutathione peroxidase 3 in non-neoplastic diseases. *Biomolecules* **14**, 689 (2024).
56. Su, H., Na, N., Zhang, X. & Zhao, Y. The biological function and significance of CD74 in immune diseases. *Inflamm Res* **66**, 209–216 (2017).
57. Sajid, M. *et al.* The functional and antiviral activity of interferon alpha-inducible IFI6 against hepatitis B virus replication and gene expression. *Front Immunol* **12**, 634937 (2021).
58. Cheriyath, V. *et al.* G1P3 (IFI6), a mitochondrial localised antiapoptotic protein, promotes metastatic potential of breast cancer cells through mtROS. *Br J Cancer* **119**, 52–64 (2018).
59. Katzengruber, L., Sander, P. & Laufer, S. MKK4 inhibitors-recent development status and therapeutic potential. *Int J Mol Sci* **24**, 7495 (2023).
60. Syc-Mazurek, S. B., Rausch, R. L., Fernandes, K. A., Wilson, M. P. & Libby, R. T. Mkk4 and Mkk7 are important for retinal development and axonal injury-induced retinal ganglion cell death. *Cell Death Dis* **9**, 1095 (2018).
61. Aging Atlas Consortium. Aging atlas: A multi-omics database for aging biology. *Nucleic Acids Res* **49**, D825–D830 (2021).
62. Song, J.-Q. *et al.* Heterozygous SOD2 deletion deteriorated chronic intermittent hypoxia-induced lung inflammation and vascular remodeling through mtROS-NLRP3 signaling pathway. *Acta Pharmacol Sin* **41**, 1197–1207 (2020).
63. Papinska, J. A., Durślewicz, J., Bagavant, H. & Deshmukh, U. S. Deleting mitochondrial superoxide dismutase 2 in salivary gland ductal epithelial cells recapitulates non-sjögren's sicca syndrome. *Int J Mol Sci* **25**, 5983 (2024).
64. Olsson, J. *et al.* Expression of neutrophil SOD2 is reduced after lipopolysaccharide stimulation: A potential cause of neutrophil dysfunction in chronic kidney disease. *Nephrol Dial Transplant* **26**, 2195–2201 (2011).
65. Liu, Y. *et al.* Genetic and functional associations with decreased anti-inflammatory tumor necrosis factor alpha induced protein 3 in macrophages from subjects with axial spondyloarthritis. *Front Immunol* **8**, 860 (2017).
66. Majumdar, I., Ahuja, V. & Paul, J. Altered expression of tumor necrosis factor alpha -

induced protein 3 correlates with disease severity in ulcerative colitis. *Sci Rep* **7**, 9420 (2017).

67. Kivimäki, M. *et al.* Social disadvantage accelerates aging. *Nat Med* **31**, 1635–1643 (2025).
68. Wei, L. *et al.* H3K18 lactylation of senescent microglia potentiates brain aging and alzheimer's disease through the NFκB signaling pathway. *J Neuroinflammation* **20**, 208 (2023).
69. Ortiz-Montero, P., Londoño-Vallejo, A. & Vernot, J.-P. Senescence-associated IL-6 and IL-8 cytokines induce a self- and cross-reinforced senescence/inflammatory milieu strengthening tumorigenic capabilities in the MCF-7 breast cancer cell line. *Cell Commun Signal* **15**, 17 (2017).
70. Li, J. *et al.* Resveratrol induces autophagy and apoptosis in non-small-cell lung cancer cells by activating the NGFR-AMPK-mTOR pathway. *Nutrients* **14**, 2413 (2022).
71. Dai, M. *et al.* LARIS enables accurate and efficient ligand and receptor interaction analysis in spatial transcriptomics. Preprint at https://doi.org/10.1101/2025.11.26.690796 (2025).
72. Ok, C. Y., Park, S., Jang, H.-O., Bae, M.-K. & Bae, S.-K. Involvement of the visfatin/toll-like receptor 4 signaling axis in human dental pulp cell senescence: Protection via toll-like receptor 4 blockade. *J Dent Sci* **18**, 1177–1188 (2023).
73. Rattanaprukskul, K. *et al.* Molecular signatures of senescence in periodontitis: Clinical insights. *J Dent Res* **103**, 800–808 (2024).
74. Zayed, M. & Iohara, K. Effects of p-cresol on senescence, survival, inflammation, and odontoblast differentiation in canine dental pulp stem cells. *Int J Mol Sci* **21**, 6931 (2020).
75. Hampel, B. *et al.* Apoptosis resistance of senescent human fibroblasts is correlated with the absence of nuclear IGFBP-3. *Aging Cell* **4**, 325–330 (2005).
76. Hong, S. & Kim, M.-M. IGFBP-3 plays an important role in senescence as an aging marker. *Environ Toxicol Pharmacol* **59**, 138–145 (2018).
77. Sugawara, T. *et al.* Claudin-11 regulates immunological barrier formation and spermatogonial proliferation through stem cell factor. *Commun Biol* **8**, 148 (2025).
78. Lizon, T. B. *et al.* Cell adhesion molecules in traumatic brain injury: Orchestrating leukocyte infiltration, BBB disruption, and neuroinflammation. *Brain, Behavior, and Immunity* **138**, 106896 (2026).
79. Duong, C. N. *et al.* Interference with ESAM (endothelial cell-selective adhesion molecule) plus vascular endothelial-cadherin causes immediate lethality and lung-specific blood coagulation. *Arterioscler Thromb Vasc Biol* **40**, 378–393 (2020).
80. Healy, J. & McInnes, L. Uniform manifold approximation and projection. *Nat Rev Methods Primers* **4**, 82 (2024).

FIGURE LEGENDS

Fig. 1 Visium HD spatial transcriptomic sequencing reveals global transcriptional changes in aged pulp and histological validation. a Schematic diagram of the Visium HD platform working principle and bin definition. **b** H&E staining of young and aged pulp tissue sections. **c** Volcano plot of differentially expressed genes in aged versus young pulp ($|\log_2 FC| > 1$, $P < 0.05$). **d–k** Cross-validation of *SELENOP*, *MMP-9*, *MMP-2*, and *TGF-β1* expression changes in young and aged pulp by immunofluorescence staining and spatial gene mapping (immunofluorescence analysis: t-test, $*P < 0.05$, $**P < 0.01$, $***P < 0.001$; spatial transcriptomic analysis: Benjamini-Hochberg test, $*P < 0.05$, $**P < 0.01$, $***P < 0.001$, $****P < 0.0001$). Scale bar: 200 μm. Data represent three young and three aged donors (n = 3 per group).

Fig. 2 Identification and spatial distribution of eight major cell types in young and aged dental pulp. a Violin plots showing the expression of marker genes for the eight cell types: *COL1A2* (fibroblasts), *NES* (progenitor cells), *VWF* (endothelial cells), *MPZ* (neural cells), *IGKC* (plasma cells), *TRBC2* (T cells), *LYZ* (monocytes), and *CD68* (macrophages). **b** Spatial transcriptomic maps showing the distribution and proportion of the eight cell populations in representative sections of young and aged pulp at 8 × 8 μm bin resolution. In young pulp, progenitor cells are enriched at the periphery of the tissue section and around blood vessels, but become mainly confined to the perivascular area after aging; immune cells show an overall reduction in aged pulp. **c** UMAP projection of all cells, colored by cell type; feature plots display the expression of specific cluster marker genes, with high expression in purple and low expression in gray. **d** Spatial mapping of the corresponding marker genes on tissue sections, validating the spatial correspondence between gene expression and cell type localization. Scale bar: 200 μm.

Fig. 3 Spatial landscape of fibroblasts. a Volcano plot of differentially expressed genes (DEGs) in fibroblasts from aged versus young pulp ($|\log_2 FC| > 0.5$, $P < 0.05$). **b** Sankey bubble diagram showing the GO pathways enriched in fibroblast DEGs and the specific genes within these pathways. **c, d** Violin plots and spatial co-expression maps showing the downregulation of the biomineral tissue development and regulation of hemopoiesis pathways in aged pulp fibroblasts. **e** UMAP projection of fibroblast subcluster analysis (16 subclusters). **f** Dot plot showing the expression of some marker genes in each subcluster. **g** Spatial mapping and pie charts showing distribution and proportion of fibroblast subclusters; subcluster 1 (*SERPINA3*/*DEPP1*) is markedly reduced in aged pulp. **h** Barplot of GO enrichment analysis of fibroblast subcluster 1 marker genes. Scale bar: 200 μm.

Fig. 4 Spatial landscape of progenitor cells. a Volcano plot of DEGs in progenitor cells from aged versus young pulp ($|\log_2 FC| > 0.5$, $P < 0.05$). **b** Sankey bubble diagram showing GO pathways enriched in progenitor cell DEGs. **c, d** Violin plots and spatial co-expression maps showing the downregulation of the regulation of fibroblast proliferation and odontogenesis pathways in aged

pulp progenitor cells. **e** UMAP projection of progenitor cell subcluster analysis (4 subclusters). **f** Dot plot showing expression of marker genes in each subcluster. **g** Spatial mapping and pie charts showing the spatial distribution and proportion of progenitor cell subclusters; subcluster 1 is markedly reduced in aged pulp. **h** Barplot of GO enrichment analysis of progenitor cell subcluster 1 marker genes. Scale bar: 200 μm.

Fig. 5 Spatial landscape of endothelial cells. a Volcano plot of DEGs in endothelial cells from aged versus young pulp ($|\log_2 FC| > 0.5$, $P < 0.05$). **b** Sankey bubble diagram showing GO pathways enriched in endothelial cell DEGs. **c, d** Violin plots and spatial co-expression maps showing the downregulation of the blood vessel development and connective tissue development pathways in aged pulp endothelial cells. **e** UMAP projection of endothelial cell subcluster analysis (3 subclusters). **f** Dot plot showing expression of marker genes in each subcluster. **g** Spatial mapping and pie charts showing distribution and proportion of endothelial cell subclusters; subcluster 1 is markedly reduced in aged pulp. **h** Barplot of GO enrichment analysis of endothelial cell subcluster 1 marker genes. Scale bar: 200 μm.

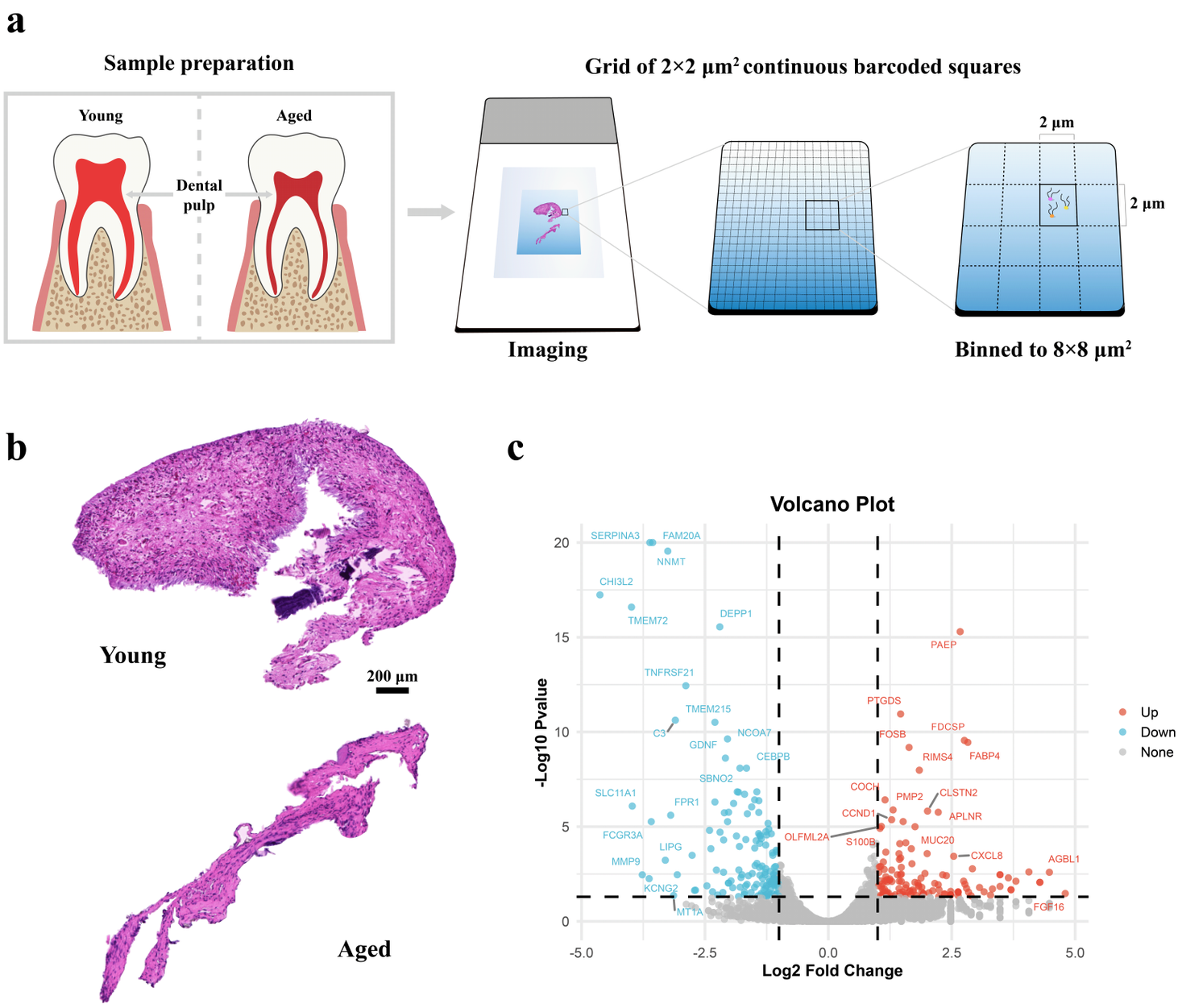
Fig. 6 Spatial landscape of neural cells. a Volcano plot of DEGs in neural cells from aged versus young pulp ($|\log_2 FC| > 0.5$, $P < 0.05$). **b** Sankey bubble diagram showing GO pathways enriched in neural cell DEGs. **c, d** Violin plots and spatial co-expression maps showing upregulation of DNA-binding transcription factor binding and downregulation of blood microparticle pathway in aged pulp neural cells. **e** UMAP projection of neural cell subcluster analysis (2 subclusters). **f** Dot plot showing expression of marker genes in each subcluster. **g** Spatial mapping and pie charts showing distribution and proportion of neural cell subclusters; subcluster 1 is slightly increased in aged pulp. **h** Barplot of GO enrichment analysis of neural cell subcluster 1 marker genes. Scale bar: 200 μm.

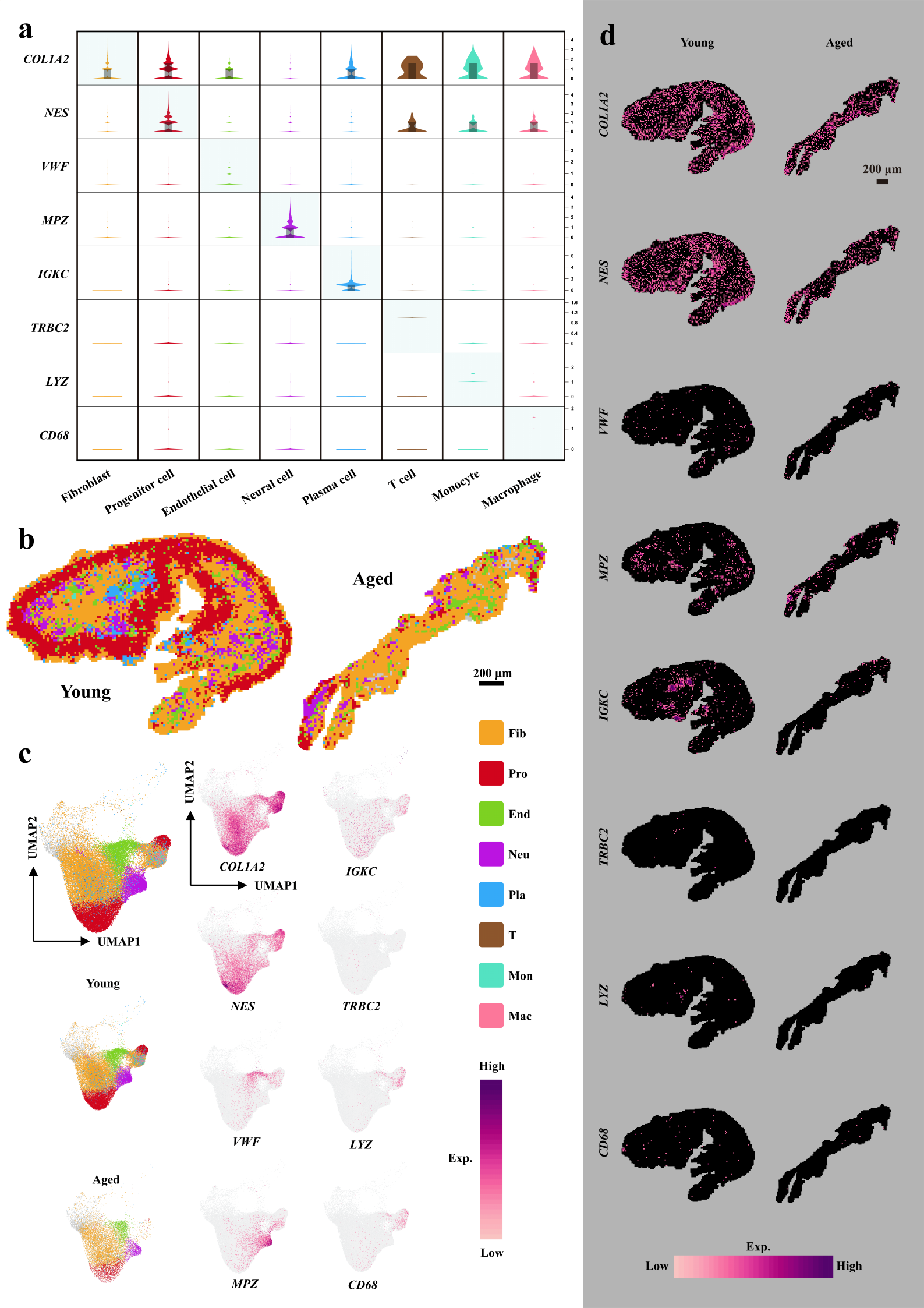
Fig. 7 Spatial landscape of immune cells. a Volcano plot of DEGs in immune cells from aged versus young pulp ($|\log_2 FC| > 0.5$, $P < 0.05$). **b** Sankey bubble diagram showing GO pathways enriched in immune cell DEGs. **c, d** Violin plots and spatial co-expression maps showing downregulation of response to growth factor and MAPK cascade pathways in aged pulp immune cells. **e** Spatial mapping and pie charts showing distribution and proportion of immune cell subclusters in aged pulp. **f** Spatial mapping of *FOS* gene on young and aged pulp tissue sections. **g** Violin plots showing downregulation of *FOS* in all four immune cell types in aged pulp. Scale bar: 200 μm.

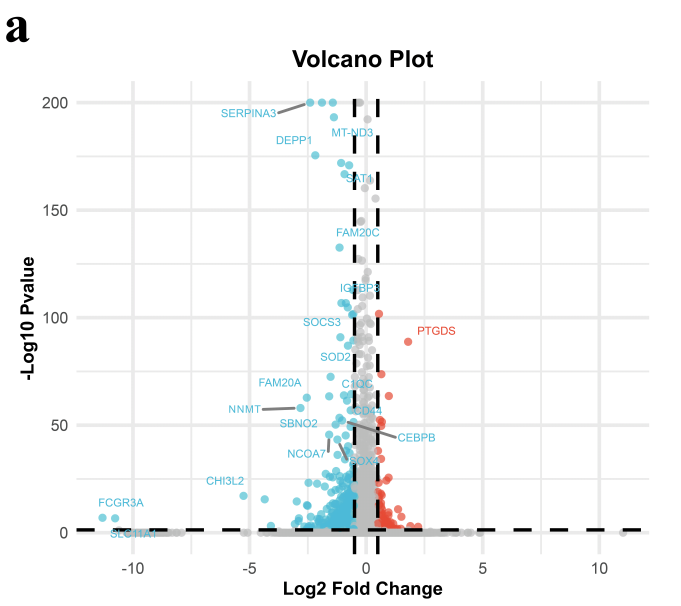
Fig. 8 Aging-related gene analysis reveals transcriptional dysregulation in aged pulp. a Venn diagram showing intersection between 272 DEGs and 503 aging-related genes (Aging Atlas), identifying 14 overlapping genes. **b** Bar chart showing 5 upregulated and 9 downregulated overlapping genes. **c** Volcano plot highlighting the 14 aging-related DEGs. **d** Bubble plot displaying expression patterns of the 14 aging-related genes. **e** Violin plot showing downregulation of *IGFBP3*

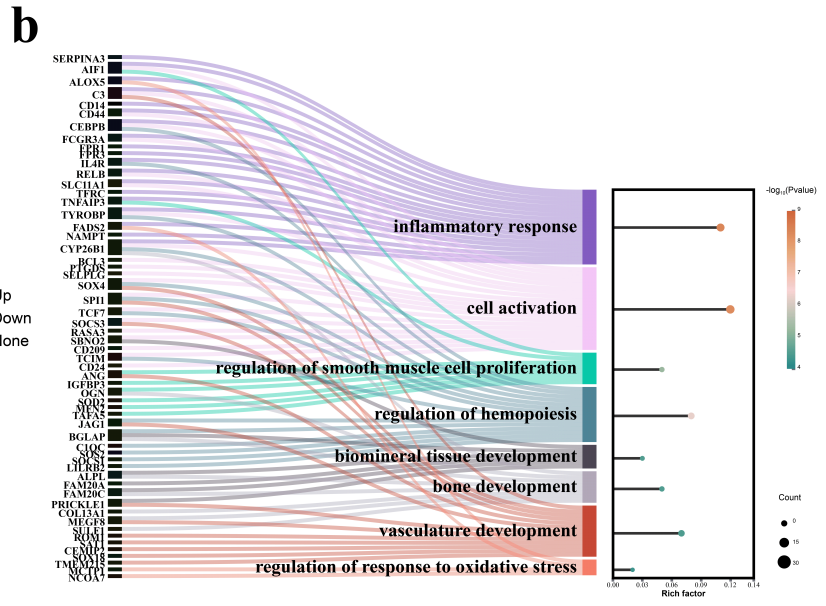
in aged pulp. **f** Spatial mapping of *IGFBP3* on pulp tissue sections. **g** Spatial distribution of progenitor cells on dental pulp tissue sections. **h** Violin plot showing expression of *IGFBP3* across cell clusters in young and aged pulp. Scale bar: 200 μm.

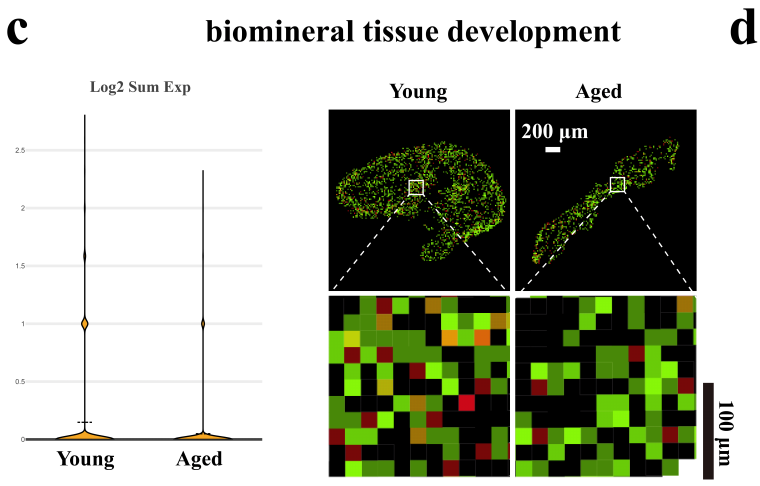
Fig. 9 LARIS cell–cell interaction analysis. a Dot plots showing sender–receiver interactions among various cell types in young and aged pulp. Dot size represents fraction of cells; red indicates high interaction score, blue low. Interaction pairs with significant differences ($P < 0.05$) are highlighted in red boxes. **b, c** Heatmaps showing number of interaction pairs among different cell types in young and aged pulp. **d** Heatmap showing difference in interaction scores between young and aged pulp. **e, f** Spatial cell distribution maps showing location of *MPZ*-expressing neural cells, fibroblasts, and plasma cells in young and aged pulp. Scale bar: 200 μm.

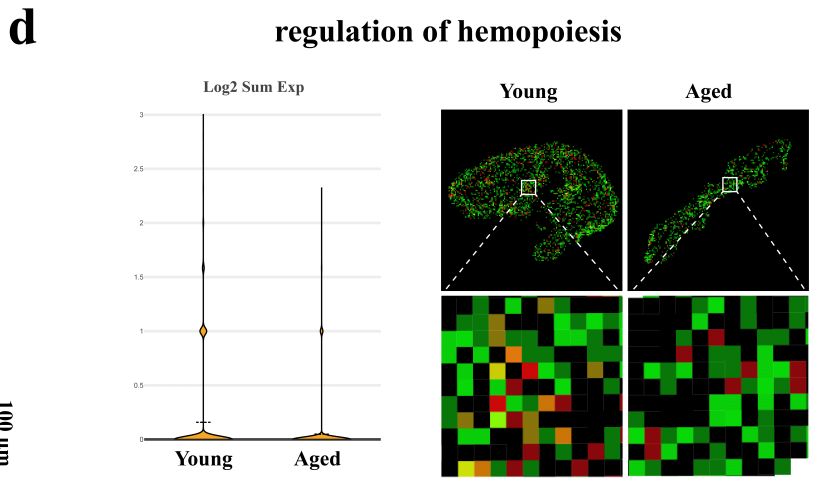

a
Sample preparation
Young
Aged
Dental pulp
Grid of 2×2 μm² continuous barcoded squares
2 μm
2 μm
Imaging
Binned to 8×8 μm²
b
Young
200 μm
Aged
c
Volcano Plot
-Log10 Pvalue
Log2 Fold Change
Up
Down
None
SERPINA3
FAM20A
NNMT
CHI3L2
TMEM72
DEPP1
PAEP
TNFRSF21
PTGDS
TMEM215
C3
NCOA7
GDNF
CEBPB
FOSB
FDCSP
RIMS4
FABP4
SBNO2
SLC11A1
FPR1
COCH
PMP2
CLSTN2
CCND1
APLNR
FCGR3A
LIPG
OLFML2A
S100B
MUC20
CXCL8
AGBL1
MMP9
KCNG2
MT1A
FGF16
d
SELENOP
Young
Aged
Positive number (%)
SELENOP
DAPI
500 μm
100 μm
e
Log2 Exp - SELENOP
Exp. SELENOP
Low
High
f
MMP9
MMP9
g
Log2 Exp - MMP9
Exp. MMP9
h
MMP2
MMP2
i
Log2 Exp - MMP2
Exp. MMP2
j
TGF-β1
TGF-β1
k
Log2 Exp - TGF-β1
200 μm
Exp. TGF-β1


a
COL1A2
NES
VWF
MPZ
IGKC
TRBC2
LYZ
CD68
Fibroblast
Progenitor cell
Endothelial cell
Neural cell
Plasma cell
T cell
Monocyte
Macrophage
b
Young
Aged
200 μm
Fib
Pro
End
Neu
Pla
T
Mon
Mac
c
UMAP2
UMAP1
Young
Aged
COL1A2
IGKC
NES
TRBC2
VWF
LYZ
MPZ
CD68
High
Exp.
Low
d
Young
Aged
200 μm
Exp.
Low
High

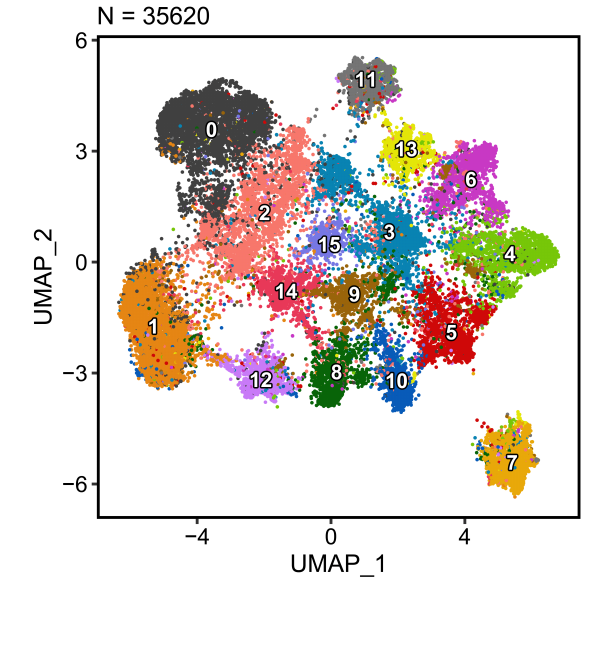

a
Volcano Plot
-Log10 Pvalue
Log2 Fold Change
SERPINA3
MT-ND3
DEPP1
SAT1
FAM20C
IGFBP3
SOCS3
PTGDS
SOD2
FAM20A
C1QC
NNMT
SBNO2
CD24
CEBPB
NCOA7
SOX4
CHI3L2
FCGR3A
SLC11A1
Up
Down
None

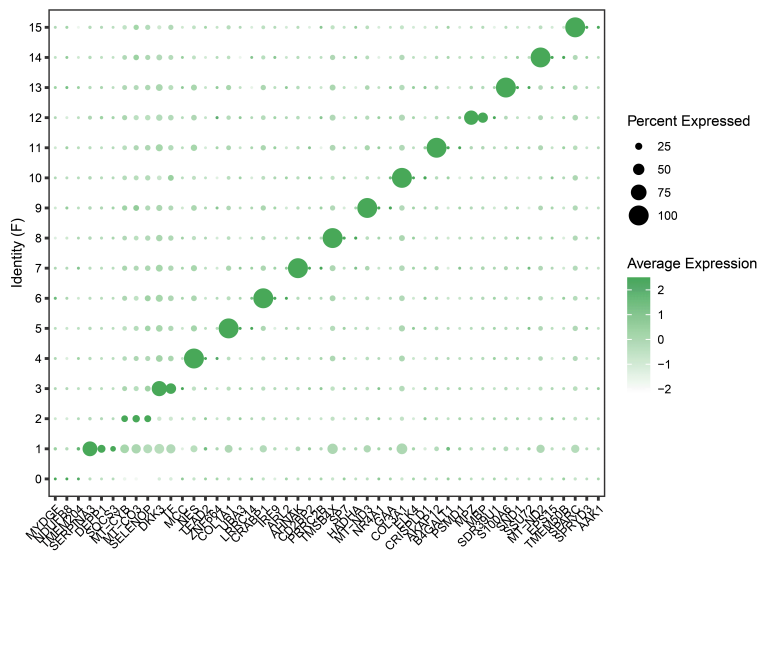

b
inflammatory response
cell activation
regulation of smooth muscle cell proliferation
regulation of hemopoiesis
biomineral tissue development
bone development
vasculature development
regulation of response to oxidative stress
Rich factor
Count

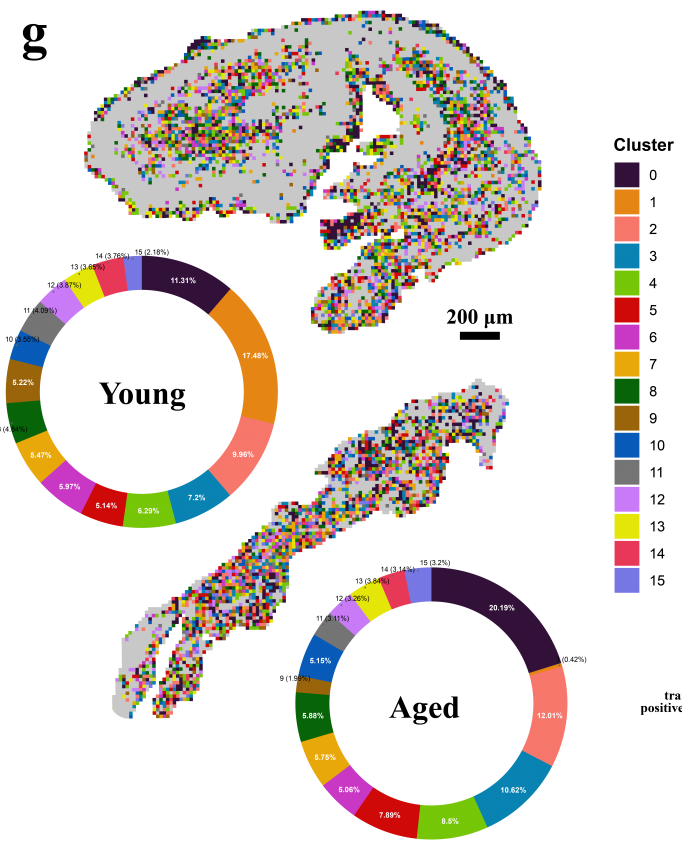

c
biomineral tissue development
Log2 Sum Exp
Young
Aged
200 μm
100 μm

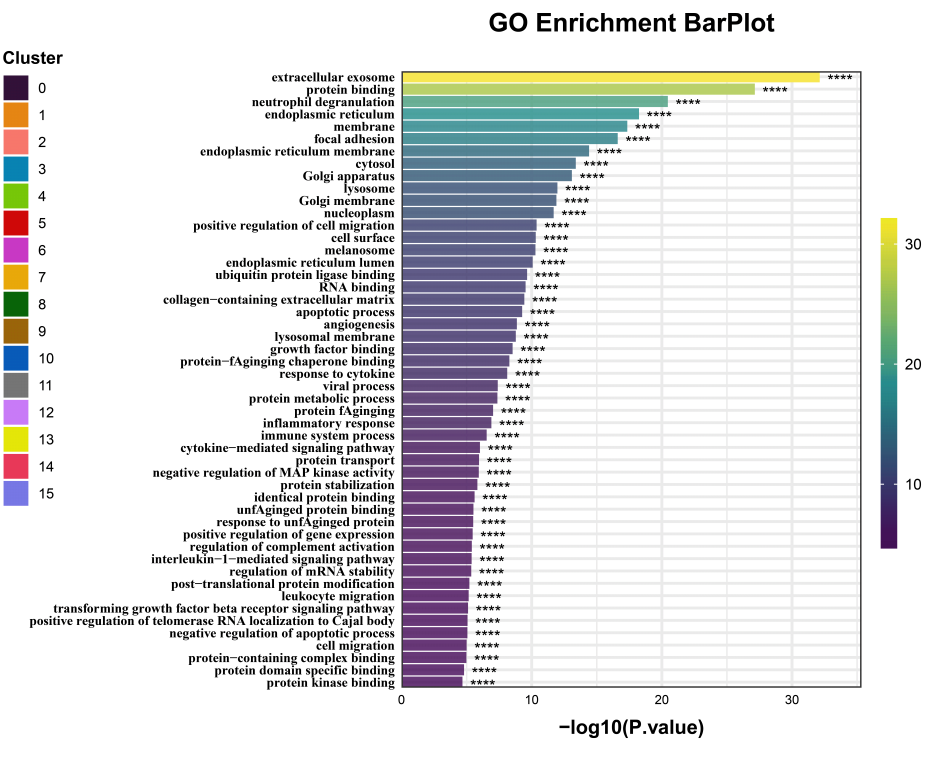

d
regulation of hemopoiesis
Log2 Sum Exp
Young
Aged

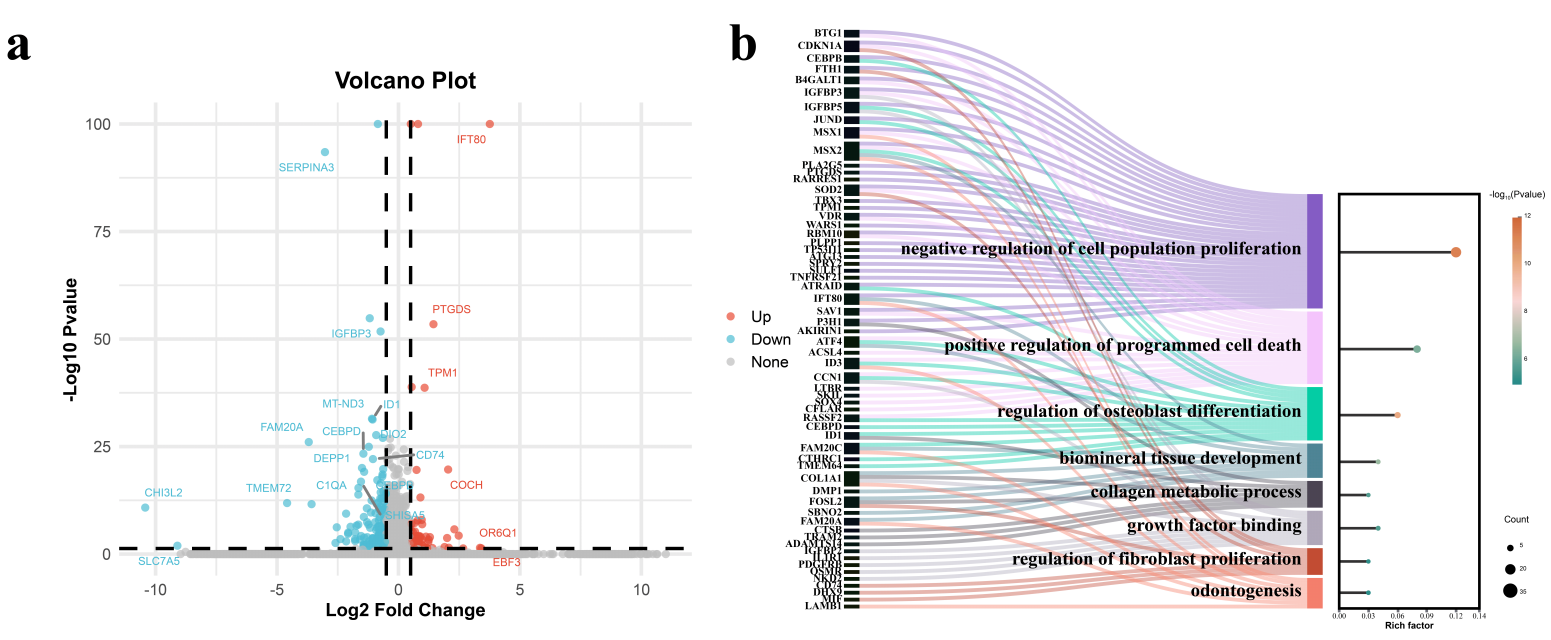

Co-expression
COL1A2
Genes in path

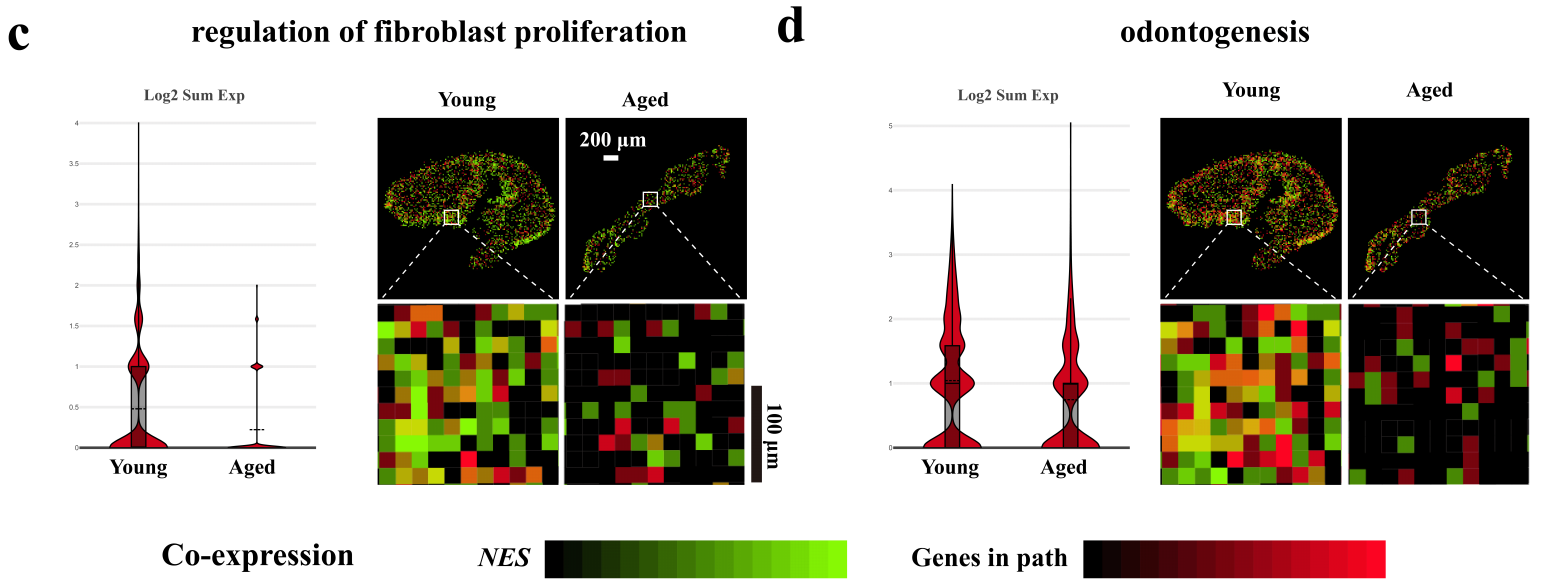

e
DP
N = 35620
UMAP_1
UMAP_2
SCT_snn_res.0.2
0(4821)
1(4706)
2(3731)
3(2869)
4(2438)
5(2077)
6(2045)
7(1973)
8(1817)
9(1572)
10(1407)
11(1370)
12(1325)
13(1317)
14(1285)
15(867)

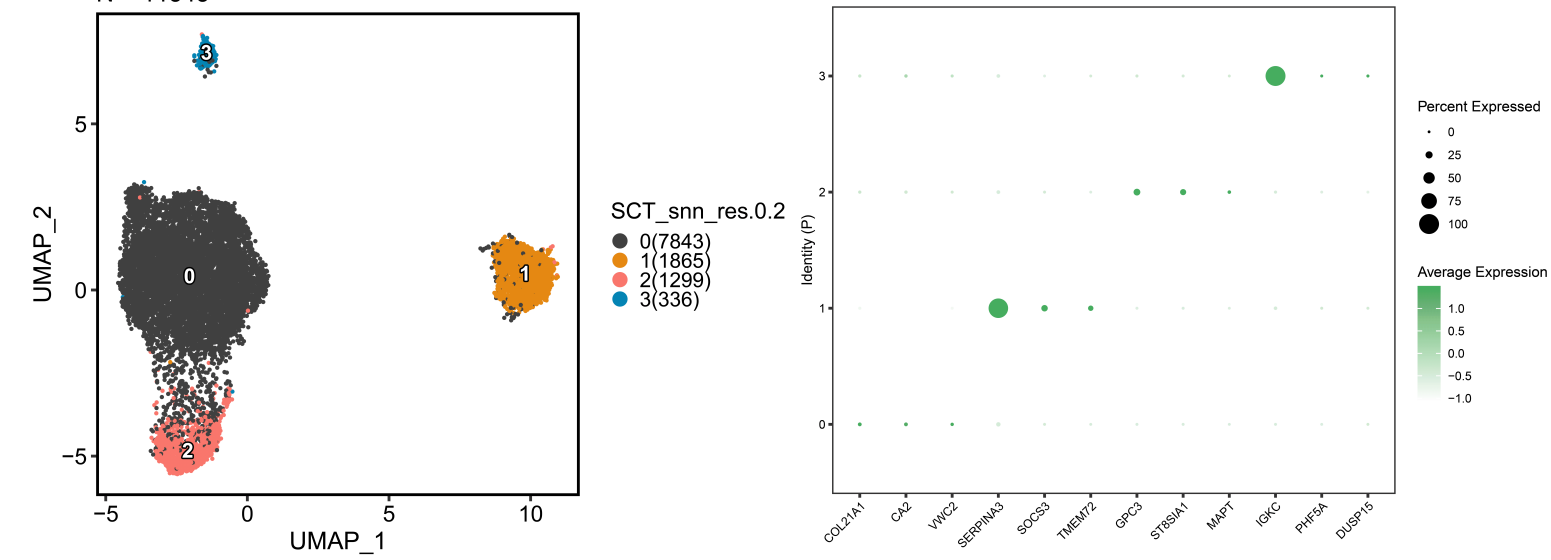

f
Identity (F)
Percent Expressed
Average Expression

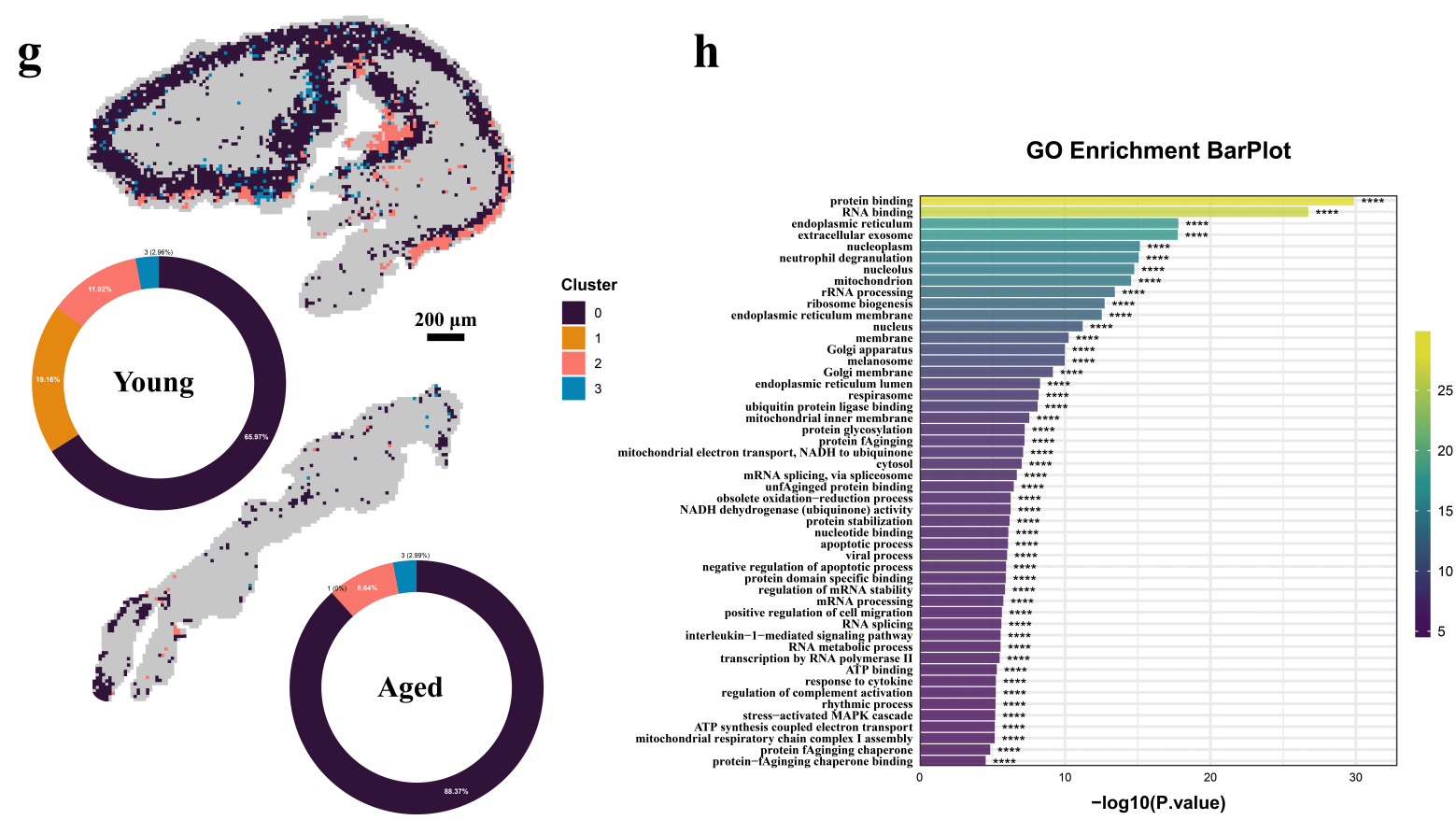

g
Cluster
Young
Aged
200 μm

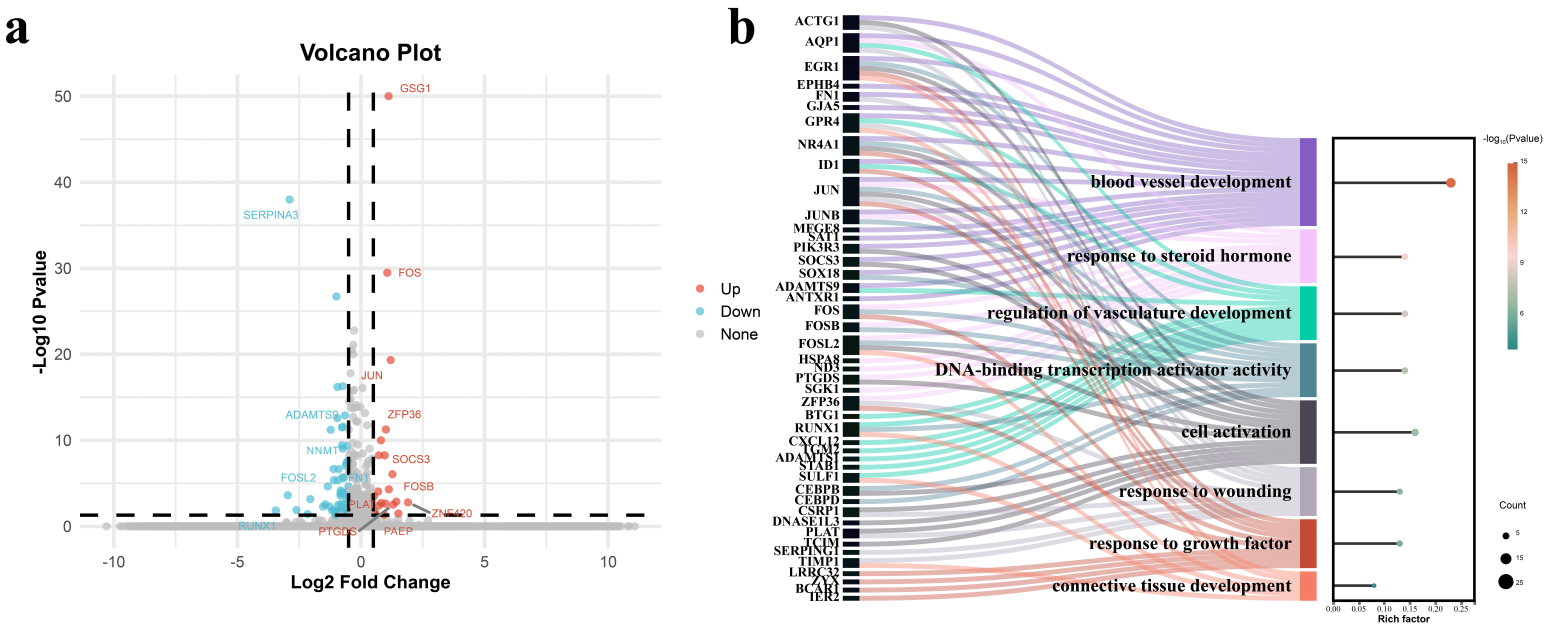

h
GO Enrichment BarPlot
extracellular exosome
protein binding
neutrophil degranulation
endoplasmic reticulum membrane
focal adhesion
cytosol
Golgi apparatus
lysosome
Golgi membrane
nucleoplasm
positive regulation of cell migration
cell surface
melanosome
endoplasmic reticulum lumen
ubiquitin protein ligase binding
RNA binding
collagen−containing extracellular matrix
apoptotic process
angiogenesis
lysosomal membrane
growth factor binding
protein−fAginging chaperone binding
response to cytokine
viral process
protein metabolic process
protein fAginging
inflammatory response
immune system process
cytokine−mediated signaling pathway
protein transport
negative regulation of MAP kinase activity
protein stabilization
identical protein binding
unfAginged protein binding
response to unfAginged protein
positive regulation of gene expression
regulation of complement activation
interleukin−1−mediated signaling pathway
regulation of mRNA stability
post−translational protein modification
leukocyte migration
transforming growth factor beta receptor signaling pathway
positive regulation of telomerase RNA localization to Cajal body
negative regulation of apoptotic process
cell migration
protein−containing complex binding
protein domain specific binding
protein kinase binding
−log10(P.value)

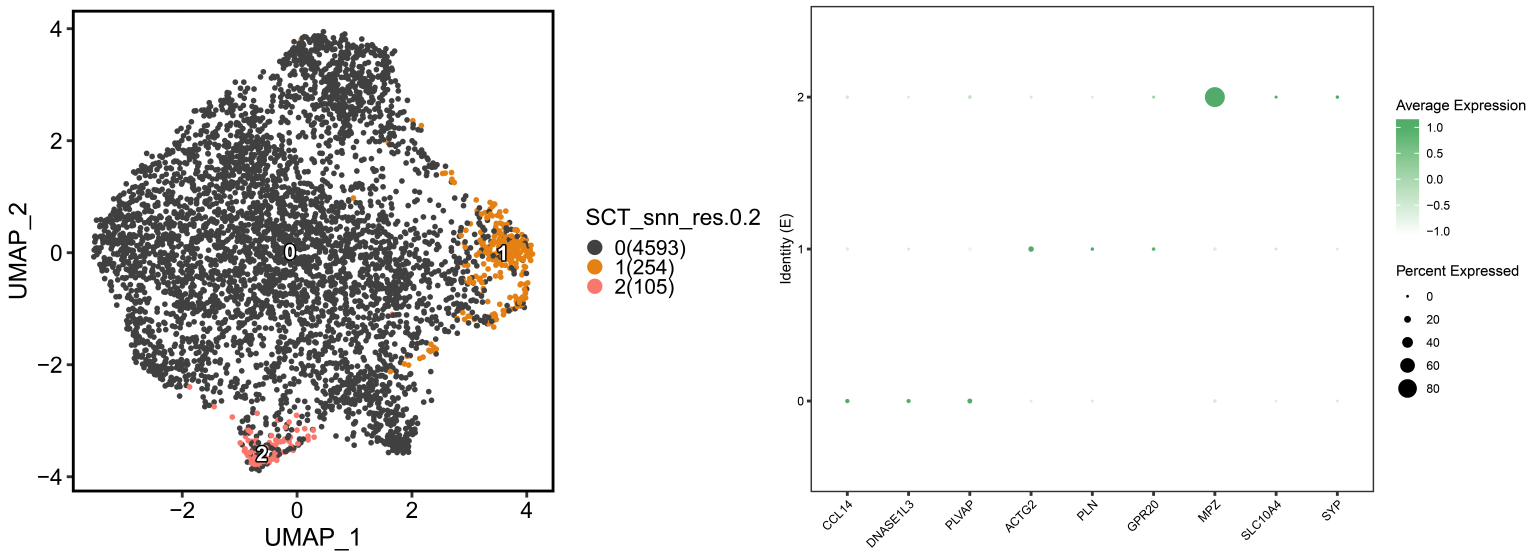

a
Volcano Plot
-Log10 Pvalue
Log2 Fold Change
IFT80
SERPINA3
PTGDS
IGFBP3
TPM1
MT-ND3
ID1
FAM20A
CEBPD
ID2
DEPP1
CD74
CHI3L2
TMEM72
C1QA
COCH
OR6Q1
EBF3
SLC7A5
b
Up
Down
None
negative regulation of cell population proliferation
positive regulation of programmed cell death
regulation of osteoblast differentiation
biomineral tissue development
collagen metabolic process
growth factor binding
regulation of fibroblast proliferation
odontogenesis
Count
Rich factor

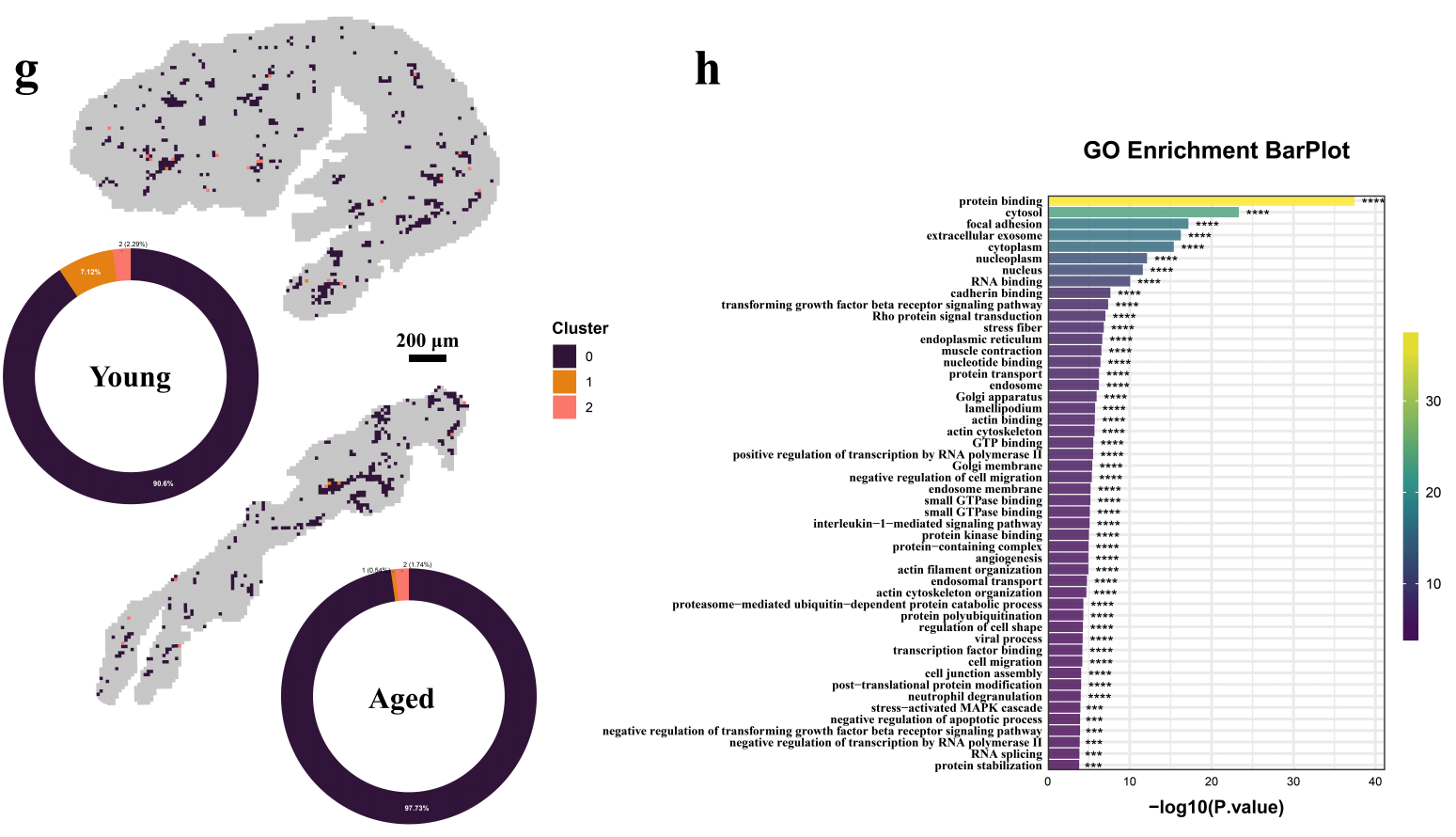

c
regulation of fibroblast proliferation
Log2 Sum Exp
Young
Aged
200 μm
100 μm
d
odontogenesis
Co-expression
NES
Genes in path

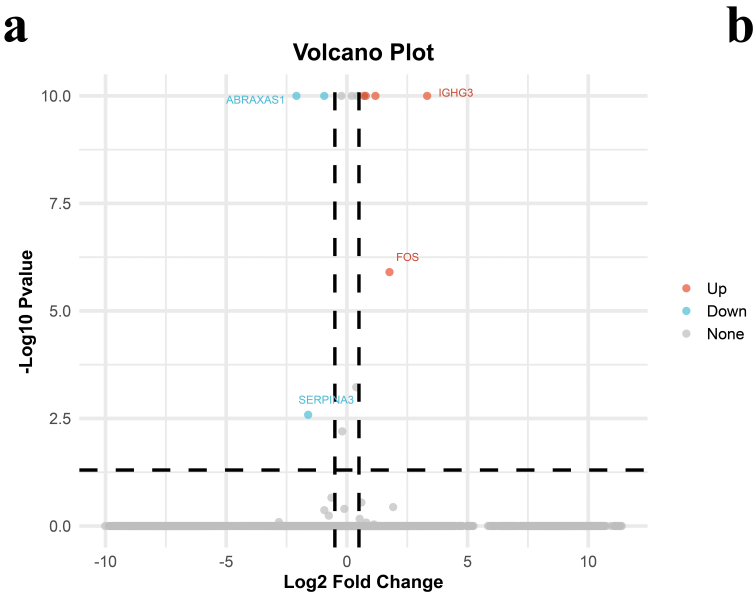

e
DP
N = 11343
UMAP_1
UMAP_2
SCT_snn_res.0.2
0(7843)
1(1865)
2(1299)
3(336)
f
Identity (P)
Percent Expressed
Average Expression
COL21A1
CA2
VWC2
SERPINA3
SOCS3
TMEM72
GPC3
ST8SIA1
MAPT
IGKC
PHF5A
DUSP15

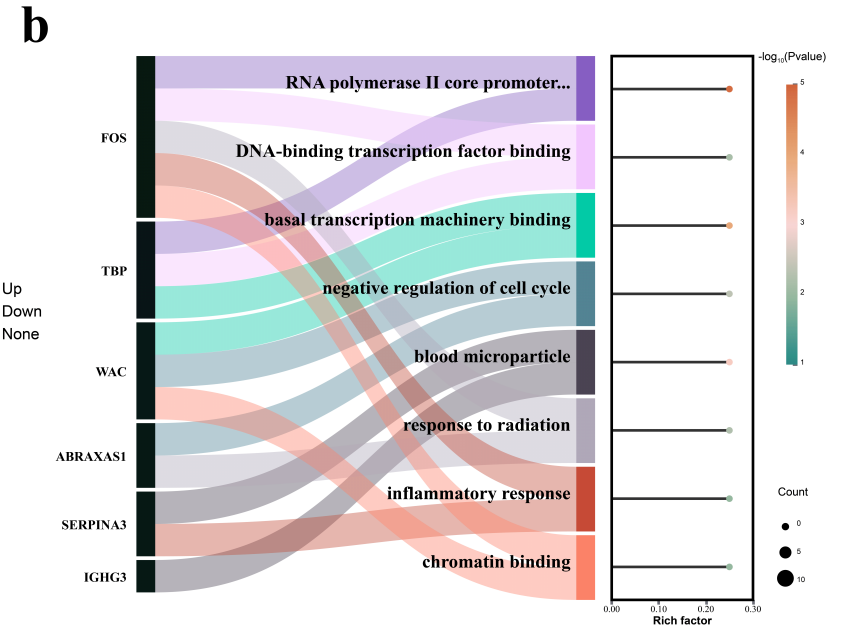

g
Cluster
0
1
2
3
200 μm
Young
Aged
h
GO Enrichment BarPlot
protein binding
RNA binding
endoplasmic reticulum
extracellular exosome
nucleoplasm
neutrophil degranulation
nucleolus
mitochondrion
rRNA processing
ribosome biogenesis
endoplasmic reticulum membrane
nucleus
membrane
Golgi apparatus
melanosome
Golgi membrane
endoplasmic reticulum lumen
respirasome
ubiquitin protein ligase binding
mitochondrial inner membrane
protein glycosylation
protein fAginging
mitochondrial electron transport, NADH to ubiquinone
cytosol
mRNA splicing, via spliceosome
unfAginged protein binding
obsolete oxidation−reduction process
NADH dehydrogenase (ubiquinone) activity
protein stabilization
nucleotide binding
apoptotic process
viral process
negative regulation of apoptotic process
protein domain specific binding
regulation of mRNA stability
mRNA processing
positive regulation of cell migration
RNA splicing
interleukin−1−mediated signaling pathway
RNA metabolic process
transcription by RNA polymerase II
ATP binding
response to cytokine
regulation of complement activation
rhythmic process
stress−activated MAPK cascade
ATP synthesis coupled electron transport
mitochondrial respiratory chain complex I assembly
protein fAginging chaperone
protein−fAginging chaperone binding
−log10(P.value)

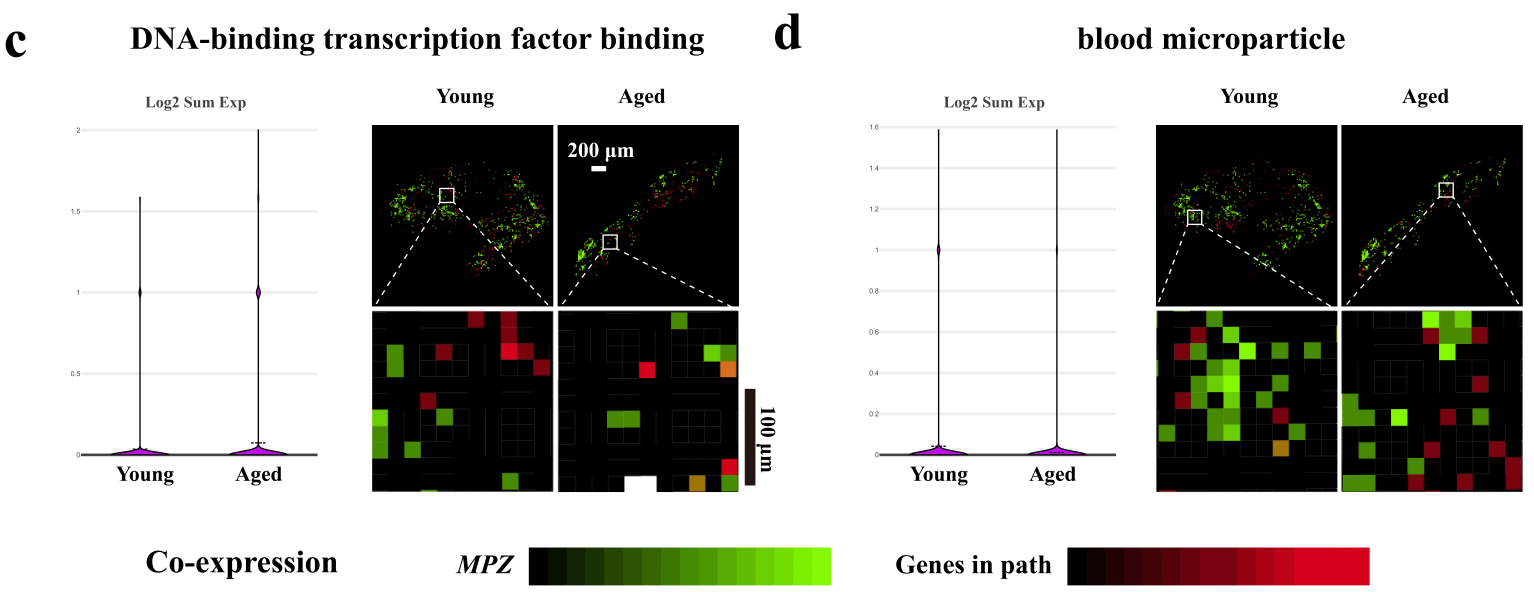

a
Volcano Plot
-Log10 Pvalue
Log2 Fold Change
GSG1
SERPINA3
FOS
JUN
ADAMTS9
ZFP36
NNMT
SOCS3
FOSL2
FOSB
RUNX1
PTGDS
PAEP
ZNF420
Up
Down
None
b
ACTG1
AQP1
EGR1
EPHB4
FN1
GJA5
GPR4
NR4A1
ID1
JUN
JUNB
MEGF8
SAT1
PIK3R3
SOCS3
SOX18
ADAMTS9
ANTXR1
FOS
FOSB
FOSL2
HSPA8
ND3
PTGDS
SGK1
ZFP36
BTG1
RUNX1
CXCL12
TCIM
ADAMTS1
STAB1
SULF1
CEBPB
CEBPD
CSRP1
DNASE1L3
PLAT
TCIM
SERPING1
TIMP1
LRRC32
CAV1
BCAM
IER2
blood vessel development
response to steroid hormone
regulation of vasculature development
DNA-binding transcription activator activity
cell activation
response to wounding
response to growth factor
connective tissue development
-log10(Pvalue)
Count
Rich factor
c
blood vessel development
Log2 Sum Exp
Young
Aged
200 μm
100 μm
d
connective tissue development
Log2 Sum Exp
Young
Aged
Co-expression
VWF
Genes in path

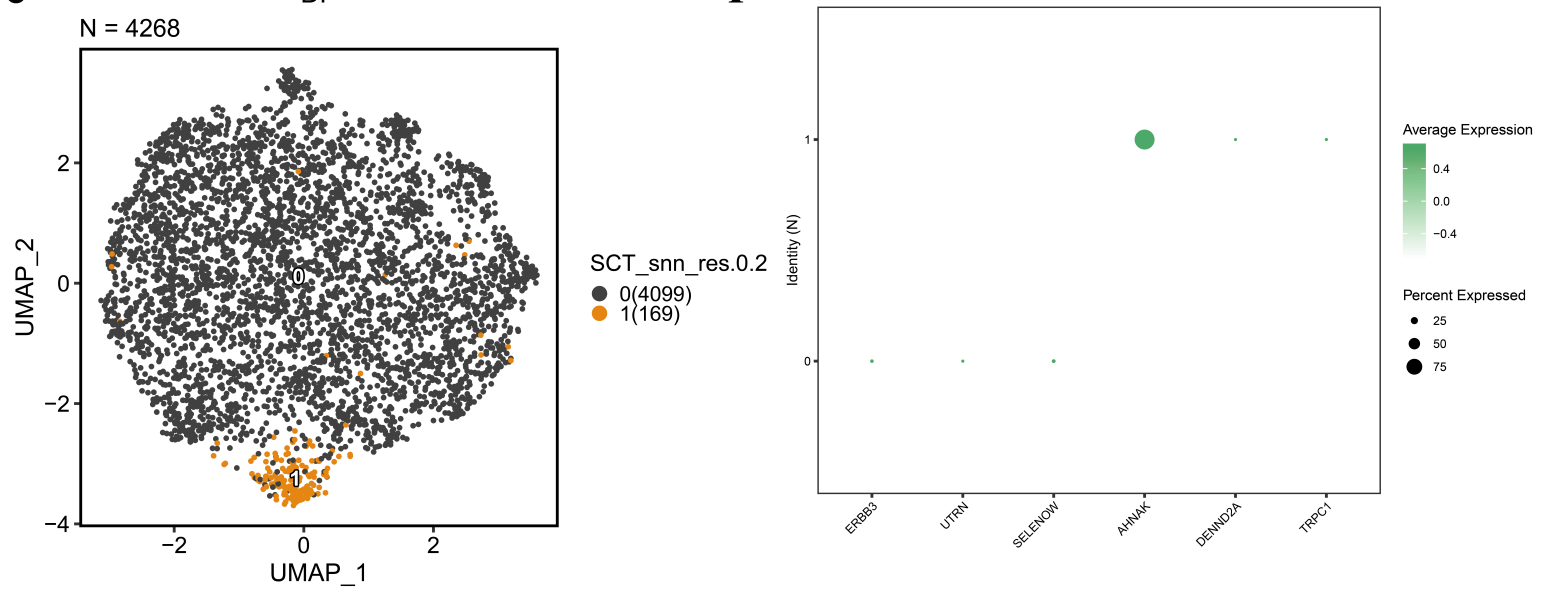

e
DP
N = 4952
UMAP_1
UMAP_2
SCT_snn_res.0.2
0(4593)
1(254)
2(105)
Identity (E)
CCL14
DNASE1L3
PLVAP
ACTG2
PLN
GPR20
MPZ
SLC10A4
SYP
Average Expression
Percent Expressed
f

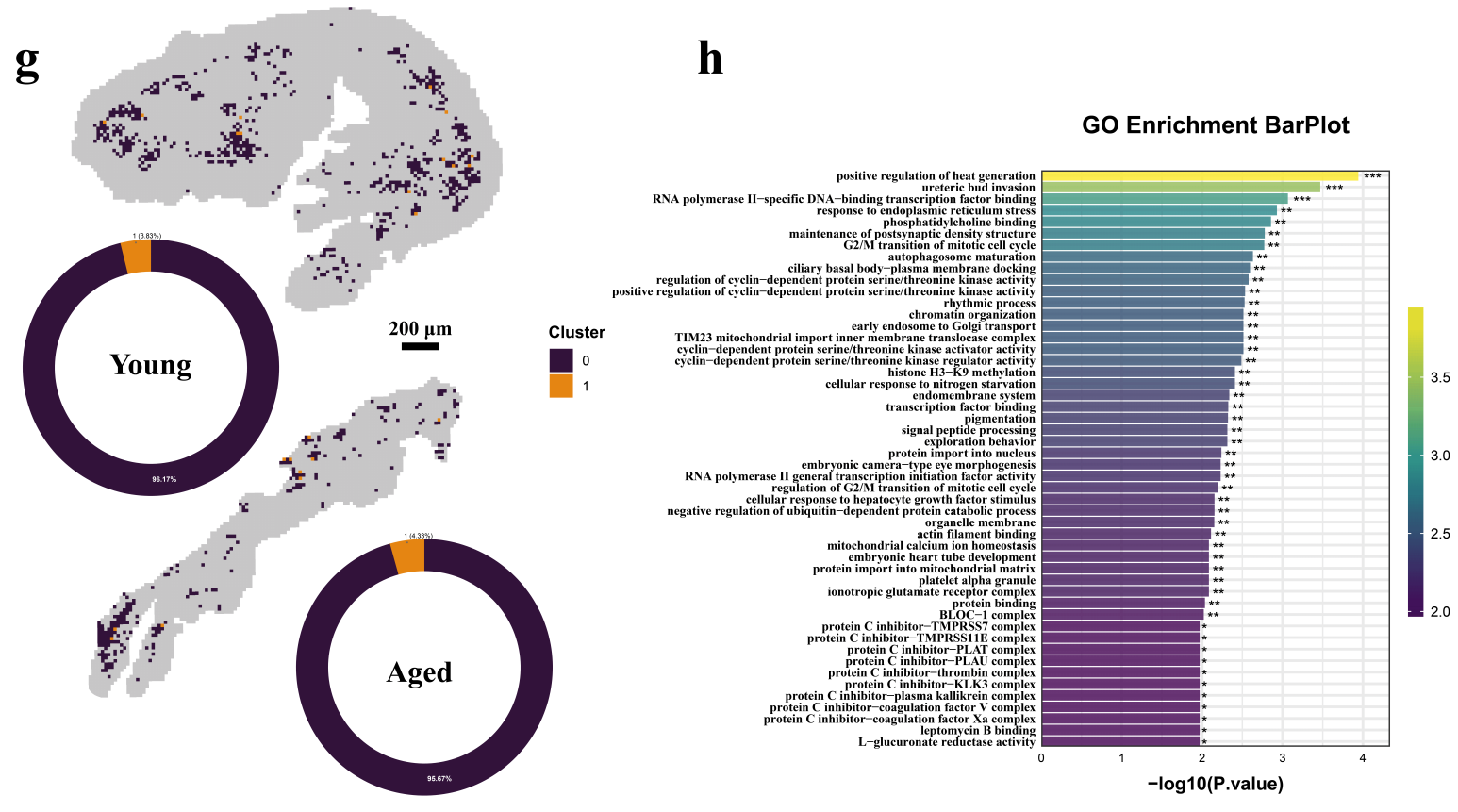

g
Young
Aged
200 μm
Cluster
0
1
2
h
GO Enrichment BarPlot
protein binding
cytosol
focal adhesion
extracellular exosome
cytoplasm
nucleoplasm
nucleus
RNA binding
cadherin binding
transforming growth factor beta receptor signaling pathway
Rho protein signal transduction
stress fiber
endoplasmic reticulum
muscle contraction
nucleotide binding
protein transport
endosome
Golgi apparatus
lamellipodium
actin binding
actin cytoskeleton
GTP binding
positive regulation of transcription by RNA polymerase II
Golgi membrane
negative regulation of cell migration
endosome membrane
small GTPase binding
small GTPase binding
interleukin−1−mediated signaling pathway
protein kinase binding
protein−containing complex
angiogenesis
actin filament organization
endosomal transport
actin cytoskeleton organization
proteasome−mediated ubiquitin−dependent protein catabolic process
protein polyubiquitination
regulation of cell shape
viral process
transcription factor binding
cell migration
cell junction assembly
post−translational protein modification
neutrophil degranulation
stress−activated MAPK cascade
negative regulation of apoptotic process
negative regulation of transforming growth factor beta receptor signaling pathway
negative regulation of transcription by RNA polymerase II
RNA splicing
protein stabilization
−log10(P.value)

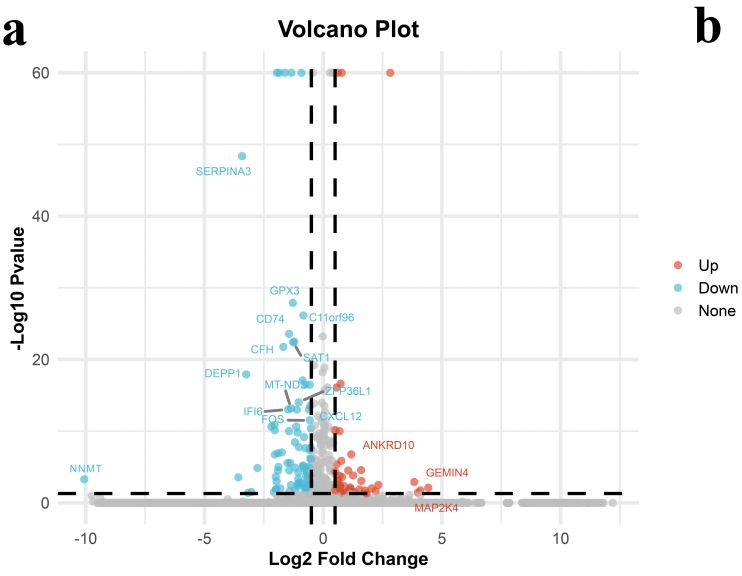

a
Volcano Plot
-Log10 Pvalue
Log2 Fold Change
ABRAXAS1
IGHG3
FOS
SERPINA3
Up
Down
None

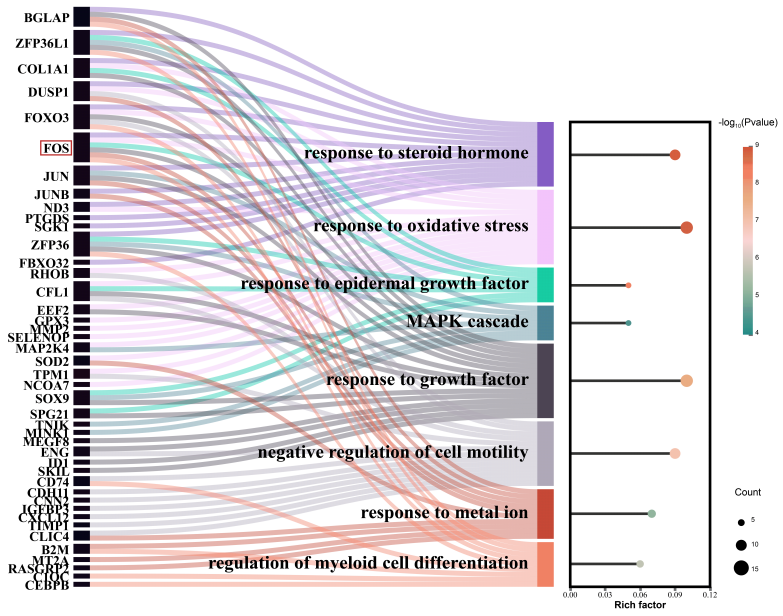

b
RNA polymerase II core promoter...
DNA-binding transcription factor binding
basal transcription machinery binding
negative regulation of cell cycle
blood microparticle
response to radiation
inflammatory response
chromatin binding
FOS
TBP
WAC
ABRAXAS1
SERPINA3
IGHG3
-log10(Pvalue)
Count
Rich factor

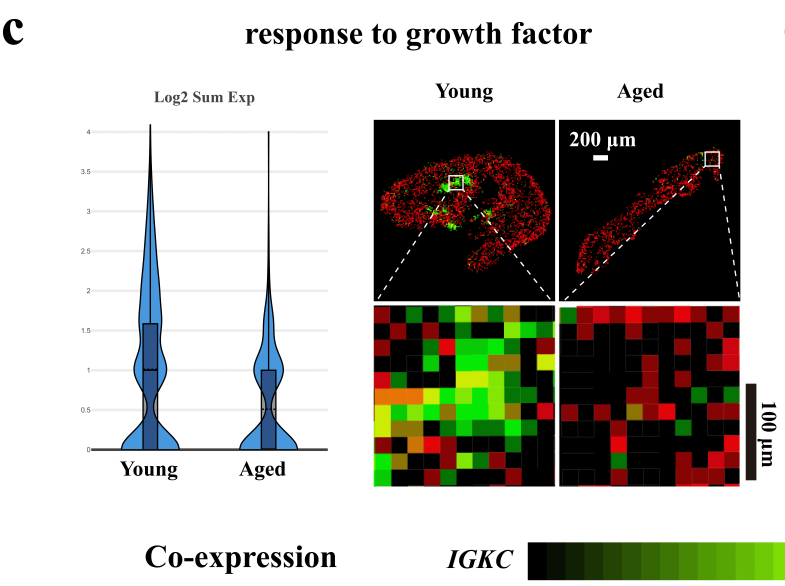

c
DNA-binding transcription factor binding
Log2 Sum Exp
Young
Aged
200 μm
100 μm
d
blood microparticle
Co-expression
MPZ
Genes in path

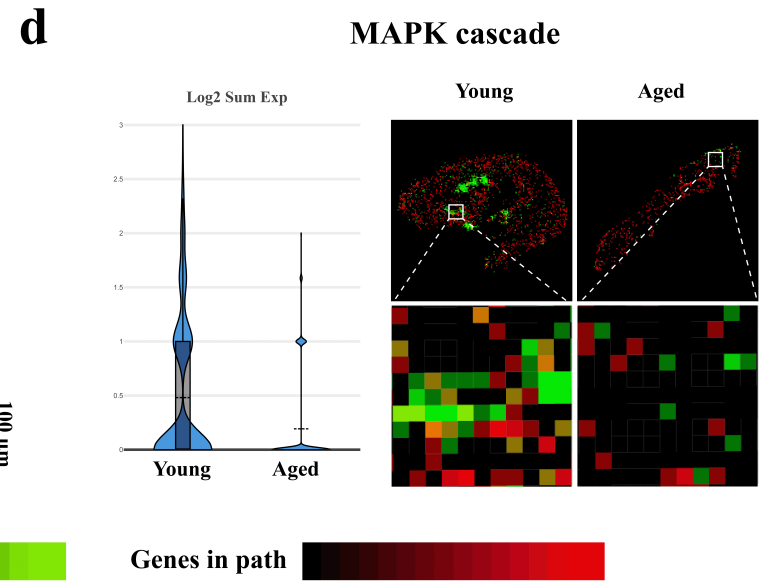

e
DP
N = 4268
UMAP_1
UMAP_2
SCT_snn_res.0.2
0(4099)
1(169)
f
Identity (N)
Average Expression
Percent Expressed
ERBB3
UTRN
SELENOW
AHNAK
DENND2A
TRPC1


g
Young
Aged
200 μm
Cluster
h
GO Enrichment BarPlot
positive regulation of heat generation
ureteric bud invasion
RNA polymerase II−specific DNA−binding transcription factor binding
response to endoplasmic reticulum stress
phosphatidylcholine binding
maintenance of postsynaptic density structure
G2/M transition of mitotic cell cycle
autophagosome maturation
ciliary basal body−plasma membrane docking
regulation of cyclin−dependent protein serine/threonine kinase activity
positive regulation of cyclin−dependent protein serine/threonine kinase activity
rhythmic process
chromatin organization
early endosome to Golgi transport
TIM23 mitochondrial import inner membrane translocase complex
cyclin−dependent protein serine/threonine kinase activator activity
cyclin−dependent protein serine/threonine kinase regulator activity
histone H3−K9 methylation
cellular response to nitrogen starvation
endomembrane system
transcription factor binding
pigmentation
signal peptide processing
exploration behavior
protein import into nucleus
embryonic camera−type eye morphogenesis
RNA polymerase II general transcription initiation factor activity
regulation of G2/M transition of mitotic cell cycle
cellular response to hepatocyte growth factor stimulus
negative regulation of ubiquitin−dependent protein catabolic process
organelle membrane
actin filament binding
mitochondrial calcium ion homeostasis
embryonic heart tube development
protein import into mitochondrial matrix
platelet alpha granule
ionotropic glutamate receptor complex
protein binding
BLOC−1 complex
protein C inhibitor−TMPRSS7 complex
protein C inhibitor−TMPRSS11E complex
protein C inhibitor−PLAT complex
protein C inhibitor−PLAU complex
protein C inhibitor−thrombin complex
protein C inhibitor−KLK3 complex
protein C inhibitor−plasma kallikrein complex
protein C inhibitor−coagulation factor V complex
protein C inhibitor−coagulation factor Xa complex
leptomycin B binding
L−glucuronate reductase activity
−log10(P.value)

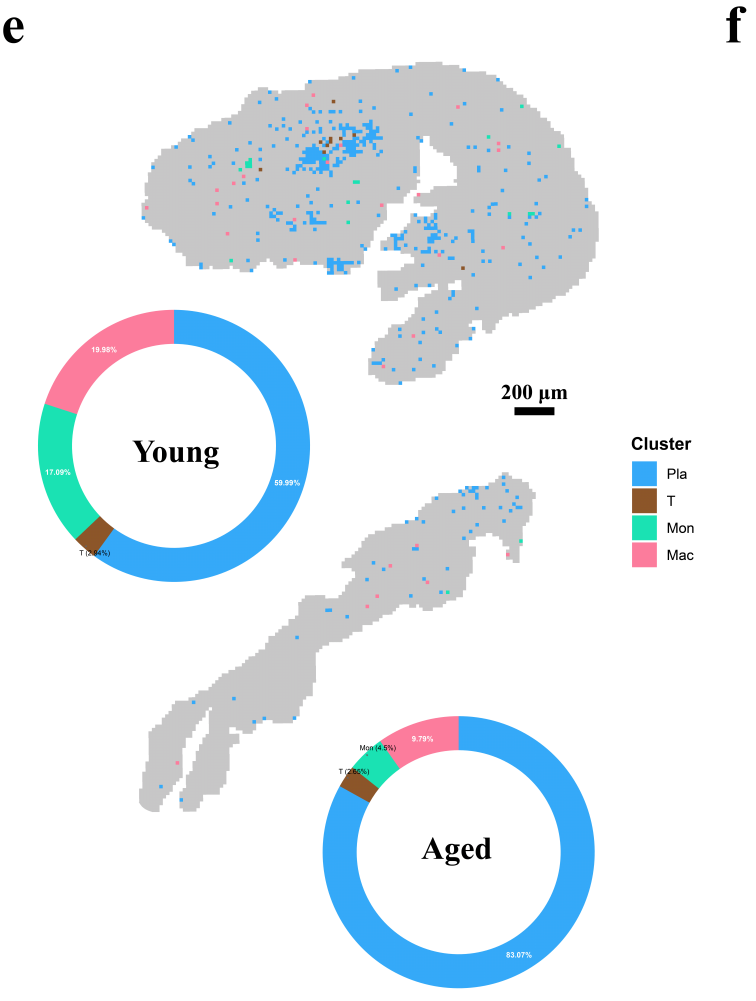

a
Volcano Plot
-Log10 Pvalue
Log2 Fold Change
Up
Down
None
SERPINA3
GPX3
CD74
C1orf96
CFH
SAT1
DEPP1
MT-ND1
ZFP36L1
IFI6
FOS
CXCL12
ANKRD10
NNMT
GEMIN4
MAP2K4

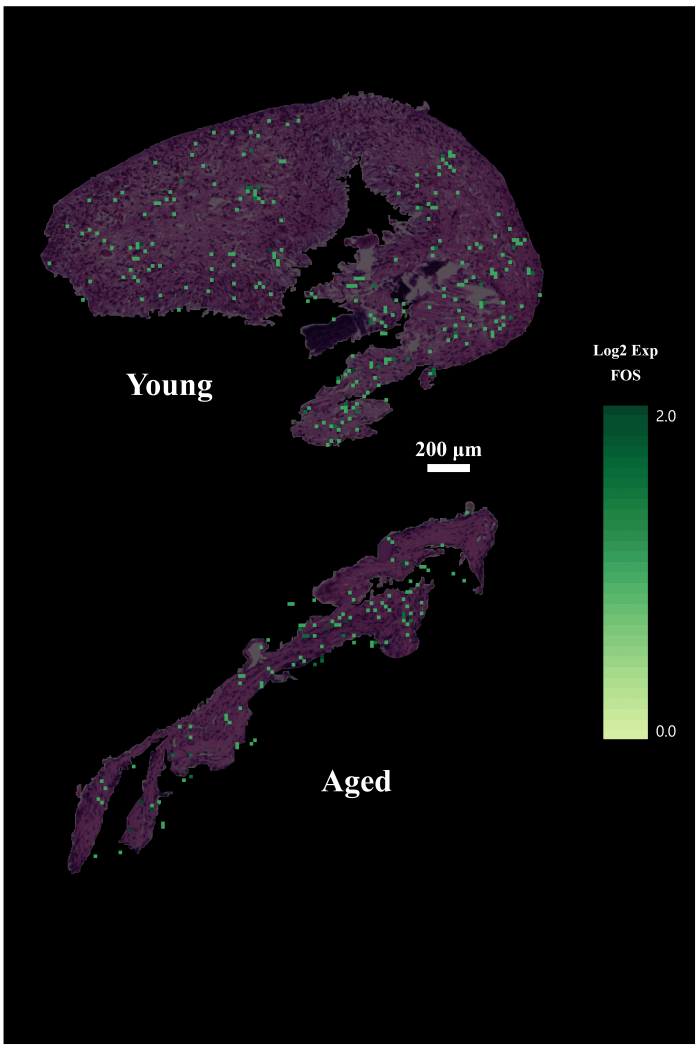

b
BGLAP
ZFP36L1
COL1A1
DUSP1
FOXO3
FOS
JUN
JUNB
ND3
PTGDS
SGK1
ZFP36
FBXO32
RHOB
CFL1
EEF2
GPX3
MMP9
SELENOP
MAP2K4
SOD2
TPM1
NCOA7
SOX9
SPG21
TNJK
MUNK1
MEGF8
ENG
IDI
SKIL
CD74
CDH11
CXCL1
IGFBP5
CXCL12
TIMP1
CLIC4
B2M
MT2A
RASGRP2
CFLAR
CEBPB
response to steroid hormone
response to oxidative stress
response to epidermal growth factor
MAPK cascade
response to growth factor
negative regulation of cell motility
response to metal ion
regulation of myeloid cell differentiation
Rich factor
Count

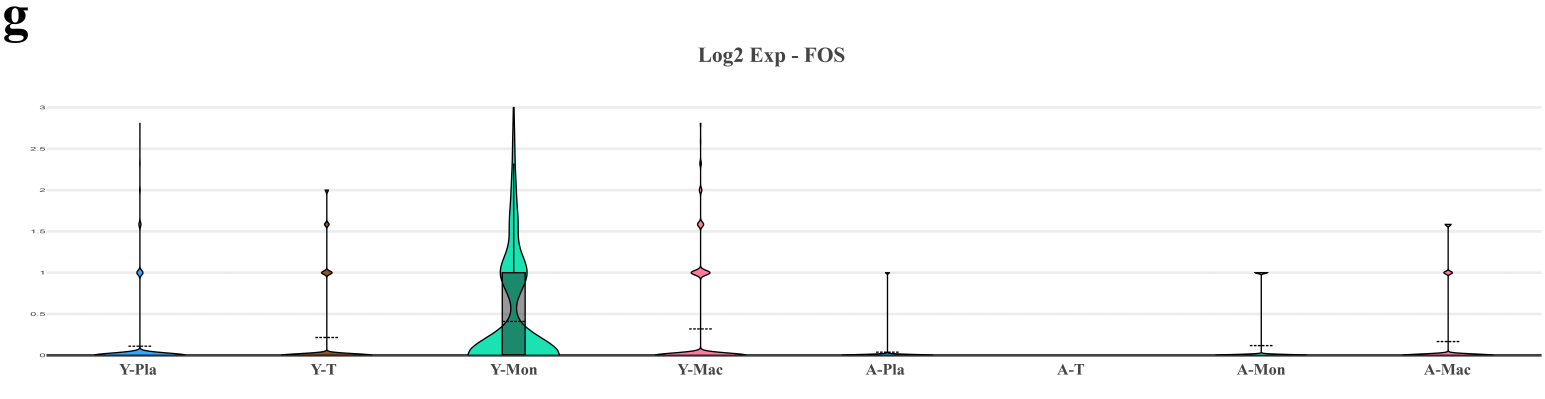

c
response to growth factor
Log2 Sum Exp
Young
Aged
200 μm
100 μm

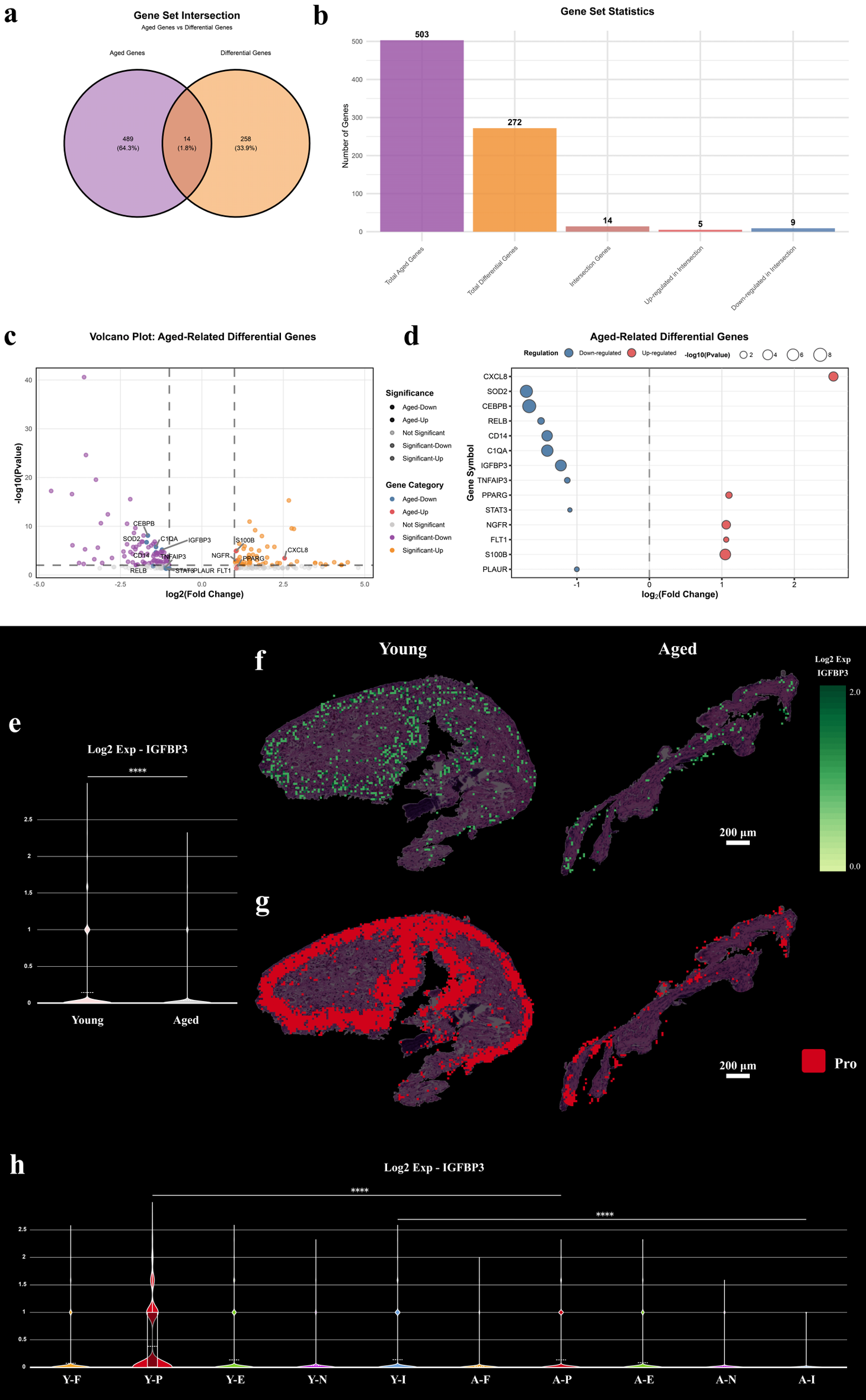

d
MAPK cascade
Log2 Sum Exp
Young
Aged

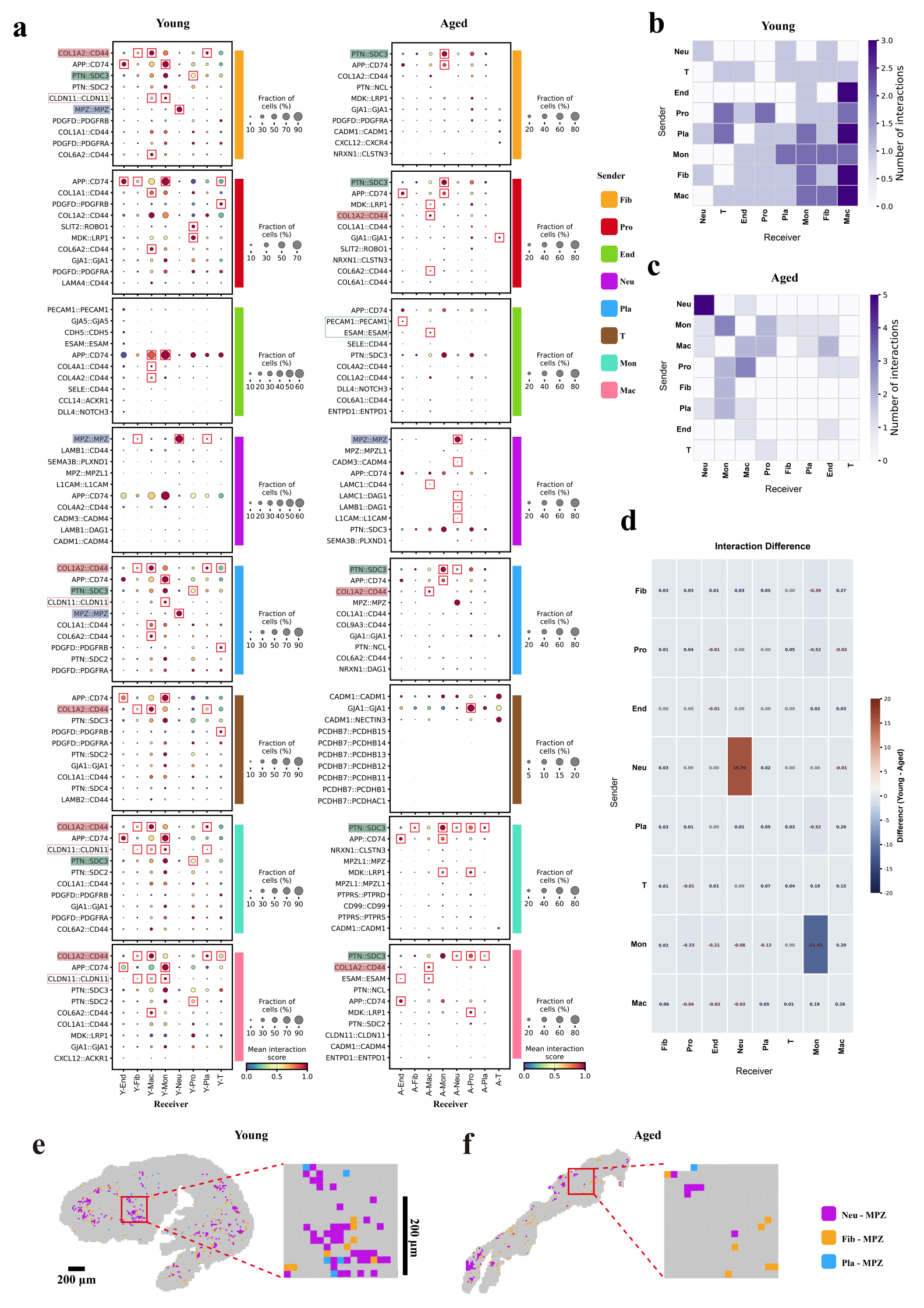
Co-expression
IGKC
Genes in path


e
Young
Aged
200 μm
Cluster
Pla
T
Mon
Mac


f
Young
Aged
200 μm
Log2 Exp
FOS
2.0
0.0


g
Log2 Exp - FOS
Y-Pla
Y-T
Y-Mon
Y-Mac
A-Pla
A-T
A-Mon
A-Mac


a
Gene Set Intersection
Aged Genes vs Differential Genes
Aged Genes
Differential Genes
489
(64.3%)
14
(1.8%)
258
(33.9%)
b
Gene Set Statistics
Number of Genes
503
272
14
5
9
Total Aged Genes
Total Differential Genes
Intersection Genes
Up-regulated in Intersection
Down-regulated in Intersection
c
Volcano Plot: Aged-Related Differential Genes
-log10(Pvalue)
log2(Fold Change)
CEBPB
SOD2
C1QA
IGFBP3
S100B
CD14
TNFAIP3
NGFR
PPARG
CXCL8
RELB
STAT3
PLAUR
FLT1
Significance
Aged-Down
Aged-Up
Not Significant
Significant-Down
Significant-Up
Gene Category
Aged-Down
Aged-Up
Not Significant
Aged-Down
Significant-Up
d
Aged-Related Differential Genes
Regulation
Down-regulated
Up-regulated
-log10(Pvalue)
Gene Symbol
log2(Fold Change)
e
Log2 Exp - IGFBP3
****
Young
Aged
f
Young
Aged
Log2 Exp
IGFBP3
2.0
0.0
200 μm
g
200 μm
Pro
h
Log2 Exp - IGFBP3
****
****
Y-F
Y-P
Y-E
Y-N
Y-I
A-F
A-P
A-E
A-N
A-I


a
Young
Aged
Sender
Fib
Pro
End
Neu
Pla
T
Mon
Mac
Fraction of cells (%)
Mean interaction score
Receiver
Y-End
Y-Fib
Y-Mac
Y-Mon
Y-Neu
Y-Pro
Y-Pla
Y-T
A-End
A-Fib
A-Mac
A-Mon
A-Neu
A-Pro
A-Pla
A-T
b
Young
Number of interactions
c
Aged
d
Interaction Difference
Differencr (Young - Aged)
e
Young
200 μm
f
Aged
Neu - MPZ
Fib - MPZ
Pla - MPZ

Supplementary Files

This is a list of supplementary files associated with this preprint. Click to download.

- Supplementaryfile.docx